

The ALMA-PILS survey: First detections of ethylene oxide, acetone and propanal toward the low-mass protostar IRAS 16293-2422

J. M. Lykke¹, A. Coutens², J. K. Jørgensen¹, M. H. D. van der Wiel¹, R. T. Garrod³, H. S. P. Müller⁴, P. Bjerkeli^{1,5}, T. L. Bourke⁶, H. Calcutt¹, M. N. Drozdovskaya⁷, C. Favre^{8,9}, E. C. Fayolle¹⁰, S. K. Jacobsen¹, K. I. Öberg¹⁰, M. V. Persson⁷, E. F. van Dishoeck^{7,11}, and S. F. Wampfler¹²

- ¹ Centre for Star and Planet Formation, Niels Bohr Institute & Natural History Museum of Denmark, University of Copenhagen, Øster Voldgade 5–7, DK-1350 Copenhagen K., Denmark
- ² Department of Physics and Astronomy, University College London, Gower St., London, WC1E 6BT, UK
- ³ Departments of Chemistry and Astronomy, University of Virginia, Charlottesville, VA 22904, USA
- ⁴ I. Physikalisches Institut, Universität zu Köln, Zùlpicher Str. 77, 50937 Köln, Germany
- ⁵ Department of Earth and Space Sciences, Chalmers University of Technology, Onsala Space Observatory, 439 92 Onsala, Sweden
- ⁶ SKA Organization, Jodrell Bank Observatory, Lower Withington, Macclesfield, Cheshire SK11 9DL, UK
- ⁷ Leiden Observatory, Leiden University, PO Box 9513, NL-2300 RA Leiden, The Netherlands
- ⁸ Université Grenoble Alpes, IPAG, F-38000 Grenoble, France
- ⁹ CNRS, IPAG, F-38000 Grenoble, France
- ¹⁰ Harvard-Smithsonian Center for Astrophysics, 60 Garden Street, Cambridge, MA 02138, USA
- ¹¹ Max-Planck Institut für Extraterrestrische Physik (MPE), Giessenbachstr. 1, 85748 Garching, Germany
- ¹² Center for Space and Habitability (CSH), University of Bern, Sidlerstrasse 5, CH-3012 Bern, Switzerland

ABSTRACT

Context. One of the open questions in astrochemistry is how complex organic and prebiotic molecules are formed. The unsurpassed sensitivity of the Atacama Large Millimeter/submillimeter Array (ALMA) takes the quest for discovering molecules in the warm and dense gas surrounding young stars to the next level.

Aims. Our aim is to start the process of compiling an inventory of oxygen-bearing complex organic molecules toward the solar-type Class 0 protostellar binary IRAS 16293-2422 from an unbiased spectral survey with ALMA, Protostellar Interferometric Line Survey (PILS). Here we focus on the new detections of ethylene oxide ($\text{c-C}_2\text{H}_4\text{O}$), acetone (CH_3COCH_3), and propanal ($\text{C}_2\text{H}_5\text{CHO}$).

Methods. With ALMA, we surveyed the spectral range from 329 to 363 GHz at $0.5''$ (60 AU diameter) resolution. Using a simple model for the molecular emission in local thermodynamical equilibrium, the excitation temperatures and column densities of each species were constrained.

Results. We successfully detect propanal (44 lines), ethylene oxide (20 lines) and acetone (186 lines) toward one component of the protostellar binary, IRAS16293B. The high resolution maps demonstrate that the emission for all investigated species originates from the compact central region close to the protostar. This, along with a derived common excitation temperature of $T_{\text{ex}} \approx 125$ K, is consistent with a coexistence of these molecules in the same gas.

Conclusions. The observations mark the first detections of acetone, propanal and ethylene oxide toward a low-mass protostar. The relative abundance ratios of the two sets of isomers, a $\text{CH}_3\text{COCH}_3/\text{C}_2\text{H}_5\text{CHO}$ ratio of 8 and a $\text{CH}_3\text{CHO}/\text{c-C}_2\text{H}_4\text{O}$ ratio of 12, are comparable to previous observations toward high-mass protostars. The majority of observed abundance ratios from these results as well as those measured toward high-mass protostars are up to an order of magnitude above the predictions from chemical models. This may reflect either missing reactions or uncertain rates in the chemical networks. The physical conditions, such as temperatures or densities, used in the models, may not be applicable to solar-type protostars either.

Key words. astrochemistry – ISM: molecules – ISM: abundances – ISM: individual object: IRAS 16293-2422

line: identification – astrobiology

1. Introduction

An important task of modern-day astrochemistry is to understand how complex organics and possible pre-biotic molecules form near young stars. The high sensitivity and angular and spectral resolution of the Atacama Large Millimeter/submillimeter Array (ALMA) enables detection of molecular species with faint emission lines in otherwise confused regions. The capabilities of ALMA were demonstrated early on by the first detection of the prebiotic molecule glycolaldehyde toward the low-

mass protostar, IRAS 16293-2422 (Jørgensen et al. 2012). This detection illustrates the potential for imaging emission from the simplest building blocks for biologically relevant molecules during the earliest stages of the Solar System on the scales where protoplanetary disks emerge, and for understanding how these molecules are formed and in what abundances. This paper presents the first detections of three such species, ethylene oxide ($\text{c-C}_2\text{H}_4\text{O}$), propanal ($\text{C}_2\text{H}_5\text{CHO}$) and acetone (CH_3COCH_3) toward IRAS 16293-2422 from an unbiased spectral survey with ALMA (Protostellar Interferometric Line Survey or PILS; Jørgensen et al. 2016).

Traditionally, detections of complex organic molecules have mostly been associated with the hot cores around high-mass pro-

Send offprint requests to: J. M. Lykke, e-mail: juliemarialykke@gmail.com

tostars toward the warm and dense central regions around such luminous sources where the molecules sublimate from the icy mantles of dust grains. Some low-mass protostars show similar characteristics on small scales; the so-called *hot corinos* (van Dishoeck & Blake 1998; Bottinelli et al. 2004; Ceccarelli 2004). A prime example of this is IRAS 16293-2422 (IRAS16293 hereafter), a protostellar Class 0 binary system, located at a distance of 120 pc (Loinard et al. 2008). IRAS16293 is perhaps the best low-mass protostellar testbed for astrochemical studies (see, e.g., Blake et al. 1994; van Dishoeck et al. 1995; Ceccarelli et al. 2000; Schöier et al. 2002). It has the brightest lines by far of all well-studied low-mass protostars and shows detections of a wealth of complex organic molecules (Cazaux et al. 2003; Caux et al. 2011). These complex organics arise in the dense gas around each of its two binary components that each show distinct chemical signatures in the warm gas on small scales resolved by (sub)millimeter wavelength aperture synthesis observations (Bottinelli et al. 2004; Kuan et al. 2004; Bisschop et al. 2008; Jørgensen et al. 2011).

To understand how these complex organic molecules form, combinations of systematic studies establishing large inventories of similar organic molecules are needed. For this purpose, structural isomers are particularly interesting since they usually share some formation and destruction pathways. The relative abundance of two such isomers may therefore provide important constraints on astrochemical models. Examples of such interesting isotope pairs are ethylene oxide and acetaldehyde as well as acetone and propanal. Ethylene oxide was first detected toward the galactic center source Sagittarius B2(N) (Sgr B2(N)) by Dickens et al. (1997; confirmed by Bellocche et al. 2013), and has since been observed in several massive star-forming regions (Nummelin et al. 1998; Ikeda et al. 2001) but so far not toward any low-mass protostar. Acetone (CH_3COCH_3), also called propanone, was the first molecule with ten atoms to be observed in the ISM. The molecule was first detected in the hot molecular core Sgr B2 (Combes et al. 1987; Snyder et al. 2002) and later in the Orion-KL star-forming region (Friedel et al. 2005; Friedel & Snyder 2008; Peng et al. 2013). It was also detected toward other massive star-forming regions (Isokoski et al. 2013) as well as toward an intermediate-mass protostar (Fuente et al. 2014). Several lines of the SMA survey of IRAS16293 were also assigned to acetone by Jørgensen et al. (2011), but it has never been properly identified in this source. More recently, it was found in material from the comet 67P/Churyumov-Gerasimenko by the COMetary Sampling And Composition (COSAC) experiment on Rosetta’s lander Philae (Goesmann et al. 2015). Propanal ($\text{C}_2\text{H}_5\text{CHO}$) has previously been detected in Sgr B2(N) by Hollis et al. (2004), where it coexists with propynal and propenal. It was also detected towards two Galactic center molecular clouds by Requena-Torres et al. (2008). Like acetone, propanal was found to be present in the comet 67P/Churyumov-Gerasimenko (Goesmann et al. 2015).

This paper presents detections of ethylene oxide, acetone and propanal toward IRAS16293 utilising a large ALMA survey at (sub)millimeter wavelength. These are all first time detections in IRAS16293 and in low-mass protostars in general. In Sect. 2, we briefly describe the observations. The identification and analysis of the data are presented in Sect. 3. Finally, we discuss the results in Sect. 4 and conclude in Sect. 5.

2. Observations

IRAS16293 was observed as part of the PILS program (PI: Jes K. Jørgensen); the survey consists of an unbiased spectral survey

covering a significant part of ALMA’s Band 7 (wavelengths of approximately 0.8 mm) as well as selected windows in ALMA’s Bands 3 (at approximately 100 GHz; 3 mm) and 6 (at approximately 230 GHz; 1.3 mm). In this paper we only utilise data from the Band 7 part of the survey (project-id: 2013.1.00278.S). An observing log, a description of the data reduction and a first overview of the data are presented in Jørgensen et al. (2016) and here we only summarize a number of the key features of the Band 7 observations.

The Band 7 part of the survey covers the frequency range from 329.15 GHz to 362.90 GHz in full. Data were obtained from both the array of 12 m dishes (typically 35–40 antenna in the array at the time of observations) and the Atacama Compact Array (ACA), or “Morita Array”, of 7 m dishes (typically 9–10 antenna in use). The pointing center was in both cases set to be a location in-between the two components of the binary system at $\alpha_{J2000} = 16^{\text{h}}32^{\text{m}}22.72^{\text{s}}$; $\delta_{J2000} = -24^{\circ}28'34''.3$. In total 18 spectral settings were observed: each setting covers a bandwidth of 1875 MHz (over four different spectral windows of 468.75 MHz wide). To limit the data-rate, the data were downsampled by a factor two to the native spectral resolution of the ALMA correlator, resulting in a spectral resolution of 0.244 MHz ($\approx 0.2 \text{ km s}^{-1}$) over 1920 channels for each spectral window. Each setting was observed with approximately 13 minutes integration on source (execution blocks of approximately 40 minutes including calibrations) for the 12 m array and double that for the ACA.

The data for each setting were calibrated and a first imaging of the continuum was performed. Thereafter, a phase-only self-calibration was performed on the continuum images and applied to the full datacubes before combining the 12 m array and ACA data and performing the final cleaning and imaging. The resulting spectral line datacubes have an root mean square (RMS) noise for the combined datasets of approximately 6–8 mJy beam $^{-1}$ channel $^{-1}$, which translates into a uniform sensitivity better than 5 mJy beam $^{-1}$ km s $^{-1}$ with beam sizes ranging from ≈ 0.4 – $0.7''$ depending on the exact configuration at the date of observation. The data used in this paper were produced with a circular restoring beam of $0.5''$ to facilitate the analysis across the different spectral windows. The conversion from Rayleigh-Jeans temperature $T_{\text{b}}[\text{K}]$ to flux density $S_{\nu}[\text{Jy/beam}]$ follows the standard formulation and T_{b}/S_{ν} ranges from 37.2 to 45.2 K Jy $^{-1}$ depending on the frequency. The resulting image cubes are strongly line-confused toward the locations of the two primary protostars. A subtraction of the continuum was therefore done statistically for each spectral window (for continuum maps and more details see Jørgensen et al. 2016). The continuum baseline for each window is found to be robust to within twice the RMS in each channel.

3. Analysis and results

Interferometric emission maps of two representative lines each for propanal, acetone, ethylene oxide, and acetaldehyde are shown in Fig. 1. The maps show emission toward both protostellar sources. Generally the lines toward IRAS16293A are approximately a factor five broader than toward IRAS16293B (e.g., Bottinelli et al. 2004; Jørgensen et al. 2011), which makes identification of individual species challenging. Consequently IRAS16293B is therefore better for separation of blended lines and identification of new species and in this paper we focus on that source. A comparison of the maps for the different molecules shows that the emission is marginally resolved toward IRAS16293B, consistent with a deconvolved extent of $\approx 0.5''$

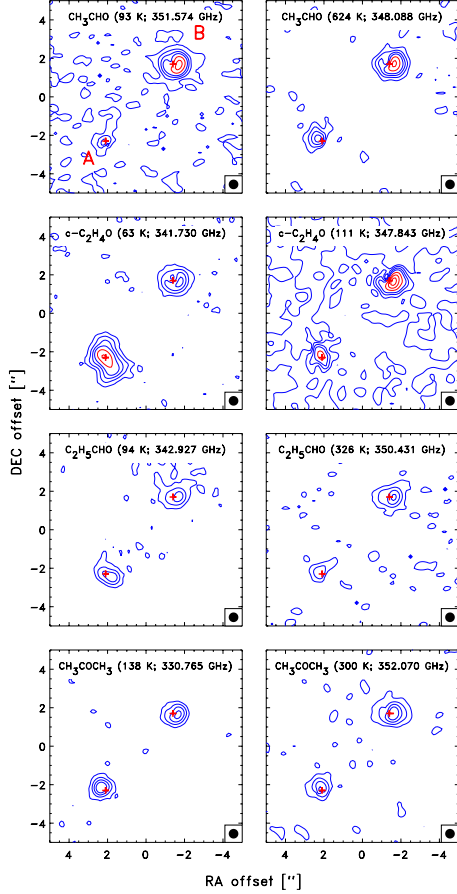


Fig. 1: Integrated intensity maps of the line emission for acetaldehyde, ethylene oxide, acetone, and propanal. Left and right columns show maps for transitions with lower and higher E_{up} , respectively. The locations of IRAS16293A (southeast) and IRAS16293B (northwest) are marked by the red plus-signs. The blue contours represent 4, 8, 12 and 16 σ while the red contours show 24, 30, 36 σ , where σ is 5 mJy beam $^{-1}$ km s $^{-1}$ for the integrated intensity. A representative beam of 0.5'' is shown in the lower right-hand corner of each panel.

toward the location of the protostar for all species. We can therefore assume that these particular molecules coexist and trace the same gas. Extracting a spectrum from the pixel located on the peak position will give the highest emission signal, but since the continuum is optically thick and very bright there are also very prominent absorption lines in the spectrum. To reduce the influence of absorption while still retaining as much intensity in the emission lines as possible, we extracted a spectrum from a position at $\alpha_{\text{J2000}} = 16^{\text{h}}32^{\text{m}}22.58^{\text{s}}$; $\delta_{\text{J2000}} = -24^{\circ}28'32''.8$, corresponding to an offset of $(-0.45''; -0.30'')$ in the southwestern direction relative to the continuum peak of IRAS16293B. This spectrum, corrected for the LSR velocity ($V_{\text{LSR}} = 2.7$ km s $^{-1}$), is used throughout this paper. Figure 2 shows the observed spectra for each of the transitions from Fig. 1.

The heavy blending of emission lines at the sensitivity of ALMA complicates the identification and analysis of individual molecular species. For this purpose we therefore calculate synthetic spectra for our target molecules and their physical parameters are derived by fitting synthetic spectra to the data. For the

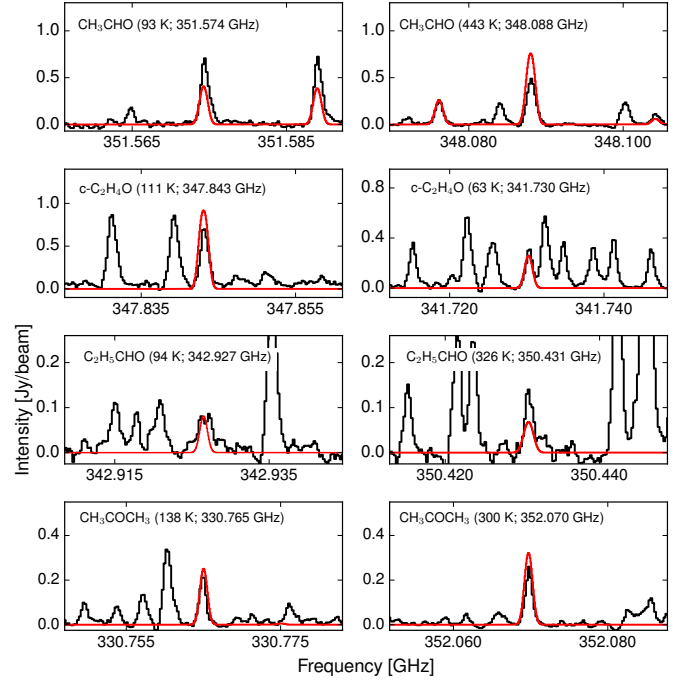


Fig. 2: Observed and synthetic spectra of the representative transitions shown in Fig. 1. The observed spectra are extracted at a position $(-0.45''; -0.30'')$ southwest of the continuum peak of IRAS16293B.

purpose of excluding blended lines from the analysis, we create a reference model containing the synthetic spectrum of emission lines of previously detected complex organic molecules that are expected to be present in the warm gas toward the two sources (Bisschop et al. 2008; Jørgensen et al. 2011, 2012, 2016; Coutens et al. 2016). Superimposing the reference model spectrum onto the observed spectrum reveals if a line of interest is blended with any of these species. For our analysis we exclude lines that are severely blended, that is, where the peaks of the emission lines overlap. In addition, we have also checked the lines of interest against other species in the CDMS¹ and JPL² databases (Müller et al. 2001, 2005; Pickett et al. 1998) with the CASSIS³ software and do not find any clear overlap with any other potential interstellar species.

The synthetic spectra are computed following the approach described in Goldsmith & Langer (1999). We assume that the molecular excitation obeys local thermodynamic equilibrium (LTE), which is reasonable at the densities and scales of the ALMA observations toward IRAS16293B (Jørgensen et al. 2016), and calculate a synthetic spectrum of all transitions from a molecule given a line width, column density, rotational temperature, and source size, assuming Gaussian line profiles. The spectroscopic data for propanal (Butcher & Wilson jr. 1964; Hardy et al. 1982; Demaison et al. 1987) and ethylene oxide (Cunningham Jr. et al. 1951; Creswell & Schwendemann 1974; Hirose 1974; Pan et al. 1998; Medcraft et al. 2012) are available from the CDMS database, while the spectroscopic data for acetone (Groner et al. 2002) and acetaldehyde (Kleiner et al. 1996) are available from the JPL database.

¹ <http://www.astro.uni-koeln.de/cdms>

² <http://spec.jpl.nasa.gov/>

³ <http://cassis.irap.omp.eu/>

For the analysis we started by identifying the brightest potential lines of each of the relevant species adopting a full width half maximum (FWHM) line width and the source size remained fixed at 1.0 km s^{-1} and $0.5''$, respectively. We then generated a synthetic spectrum by adjusting the temperature and column density (N_{tot}) until a good fit for those lines was obtained. From this a priori spectrum, we identified approximately ten reasonably non-blended and optically thin ($\tau \leq 0.1$) lines for each species, which we use to minimize the reduced chi-squared statistic:

$$\chi_{\text{red}}^2 = \frac{1}{N} \sum_{i=1}^N \left(\frac{I_{\text{obs},i} - I_{\text{syn},i}}{\sigma_i} \right)^2, \quad (1)$$

where I_{obs} and I_{syn} are the intensities of the observed and synthetic emission lines, respectively, N is the number of lines analyzed and σ the RMS error. In the analysis, we varied the column density from $1.0 \times 10^{14} \text{ cm}^{-2}$ – $1.0 \times 10^{18} \text{ cm}^{-2}$ with small increments and the temperature from 100 K – 400 K with increments of 25 K, generating a new synthetic spectrum at each increment to evaluate against the observed spectrum at the locations of the chosen lines. Since the emission lines are blended, the reduced χ^2 is only calculated for the average value of the channels at the very peak of the lines (corresponding to the predicted frequency of the peak $\pm 0.25 \text{ MHz}$), instead of over the entire Gaussian bell curve.

From the reduced χ^2 analysis, acetaldehyde and ethylene oxide show the best fit at $T_{\text{ex}} \approx 125 \text{ K}$, while it is difficult to constrain the excitation temperature for propanal and acetone. Our analysis shows that the column densities do not vary greatly with temperature for all species, except for acetone, where a $T_{\text{ex}}=400 \text{ K}$ results in a column density a factor of ten higher than for $T_{\text{ex}}=100 \text{ K}$. A comparison between the synthetic and observed spectrum for acetone reveals that an excitation temperature of approximately 200 K could still be in agreement with the observations, but that a T_{ex} of 300 K overproduces some of the lines. Since it appears that the molecules are spatially coexisting and trace the same gas, we therefore assume $T_{\text{ex}} = 125 \text{ K}$ for all molecules. The resulting column densities are summarized in Table 1 and the relative abundance ratios of the different isomers are listed in Table 2. The uncertainties of T_{ex} and N_{tot} are dominated by the assumptions that go into the analysis, that is, LTE and Gaussian line profiles, instead of the statistical error. Therefore, the uncertainties are estimated to $\sim 50\%$ and 25 K on the column density and the emission temperature, respectively.

Figs. A.1–A.19 in the Appendix show the synthetic spectra of ethylene oxide, propanal, and acetone, respectively, as well as the reference model superimposed on the observed spectrum for all lines where the synthetic spectrum predicts a peak line intensity equal to or above twice the RMS noise of the spectrum. The lines are sorted into descending intensity. We check each line in the synthetic spectra against the observed spectrum for each molecule, and the majority of them provide a reasonable match, within the estimated uncertainty. We claim a detection for lines *i*) that are reasonably well separated from other species in the reference model and *ii*) where the integrated line strength over FWHM is larger than three times the statistical uncertainty ($\sqrt{n_{\text{chan}}} \times \text{RMS}$) of the line and *iii*) where there is a reasonably good fit between the synthetic and the observed spectrum. Table B.1 in the appendix lists the spectroscopic catalog values, the integrated intensity over the FWHM for the observed spectrum, and the detection level for the detected lines of ethylene oxide, propanal, and acetone. The transitions are listed with

Table 1: Best fit column densities

Molecule		$N_{\text{tot}} [\text{cm}^{-2}]$
Acetone	CH_3COCH_3	1.7×10^{16}
Propanal	$\text{C}_2\text{H}_5\text{CHO}$	2.2×10^{15}
Acetaldehyde	CH_3CHO	7.0×10^{16}
Ethylene oxide	$\text{c-C}_2\text{H}_4\text{O}$	6.1×10^{15}

Notes. The results are derived assuming $\theta_{\text{source}} = 0.5''$, $T_{\text{ex}} = 125 \text{ K}$ and $\text{FWHM} = 1.0 \text{ km s}^{-1}$. The column density of propanal was corrected by a factor of 1.489 to take into account the vibrational and conformational contribution at $T = 125 \text{ K}$.

increasing frequency and it should be noted that many of the detected lines are a blend of several internal rotation components.

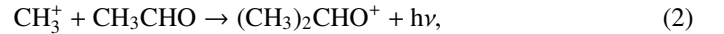
For ethylene oxide, propanal, and acetone, we detected 20, 44, and 186 lines, respectively. Some of the acetone lines predicted by the models appear to be either slightly shifted or missing. In some cases, this can be explained by the presence of absorption at the same frequency as the predicted lines, but in most cases these lines correspond to transitions with both high K_a and low K_c quantum numbers (see Table C.1). None of the missing or shifted lines with high K_a and low K_c numbers were used for the determination of the spectroscopic parameters. It was admitted by Groner et al. (2002) that these lines do not fit very well. It could be due to perturbations from interactions between the (high K_a , low K_c) levels and the levels from the lowest torsional excited states (Groner et al. 2002).

We also search for vinyl alcohol (Saito 1976), another isomer of acetaldehyde and ethylene oxide, but no detection can be claimed so far. With a conservative upper limit of $2 \times 10^{15} \text{ cm}^{-2}$ for the syn form (the lowest energy form of vinyl alcohol), this isomer is less abundant than acetaldehyde and ethylene oxide, similarly to what was found in Sgr B2 by Belloche et al. (2013).

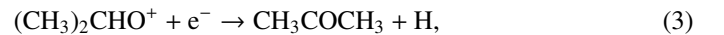
4. Discussion

As described in the introduction, the relative abundances of the different isomers are important constraints on chemical models and provide insight into the formation of the complex species. Table 2 lists the different abundance ratios and Fig. 3 gives a schematic overview of the entries from the table. A number of different formation pathways have been proposed for the studied species.

For acetone, the ion-molecule radiative association reaction

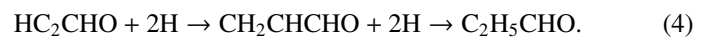


followed by



proposed by Combes et al. (1987) has been shown not to be efficient enough to produce the observed values (Herbst et al. 1990). In the model presented by Garrod et al. (2008), acetone is formed on grains by the addition of CH_3 to CH_3CO .

Hollis et al. (2004) proposed the formation of propanal to occur through simple successive hydrogenation:



However, Garrod (2013) proposed a different formation route through the addition of HCO and C_2H_5 radicals on grains. Garrod (2013) found the formation to be most rapid at 30 K, when sublimation of grain-surface methane (CH_4) is most efficient.

Table 2: Relative abundances in different sources

Source	$\text{CH}_3\text{COCH}_3 / \text{C}_2\text{H}_5\text{CHO}$	$\text{CH}_3\text{CHO} / \text{c-C}_2\text{H}_4\text{O}$	References
IRAS16293-2422	8	12	this study
Sgr B2(N)	$\geq 3.6 - 14.5^{(a)}$	$3.7 - 7.4^{(b)}$	Belloche et al. (2013)
Survey of massive SF regions	–	1.2 – 13.2	Ikeda et al. (2001)
Chemical model: peak gas-phase	0.22: 0.83: 0.07 ^(c)	–	Garrod (2013)
Chemical model: peak grain-surface	0.37: 2.3: 0.39 ^(c)	–	Garrod (2013)
Chemical model of hot cores	–	1 ^(d)	Occhiogrosso et al. (2014)

Notes. ^(a) Range reflects span for rotational states in the $V_{\text{off}} = 0 \text{ km s}^{-1}$ and the $V_{\text{off}} = 10 \text{ km s}^{-1}$ components of Sgr B2(N). Propanal is not detected, therefore the upper limit is used after correction for a similar beam filling factor. ^(b) Range reflects span for the rotational and first torsionally ($v_t=1$) excited states of acetaldehyde in the $V_{\text{off}} = -1 \text{ km s}^{-1}$ component of Sgr B2(N). ^(c) Chemical model of hot cores for a slow, medium, and fast model, respectively. ^(d) The MONACO code (at 200 K and 1.2×10^6 yrs).

Laboratory experiments were conducted by Bennett et al. (2005a,b) to study the synthesis of acetaldehyde, ethylene oxide, and vinyl alcohol in interstellar and cometary ices after irradiation with energetic electrons. Acetaldehyde appeared to be formed in both CO-CH_4 and $\text{CO}_2\text{-C}_2\text{H}_4$ ice mixtures, while ethylene oxide and vinyl alcohol are only detected in $\text{CO}_2\text{-C}_2\text{H}_4$ ice mixtures (Bennett et al. 2005a,b). While CO, CO_2 , and CH_4 have been observed in interstellar ices, C_2H_4 is formed as a secondary product by charged particle irradiation and photolysis of CH_4 ices and it is therefore likely only present in small concentrations (Bennett et al. 2005b) although it may be formed through gas-phase mechanisms under cold, dense conditions. Thus, assuming the relative production rates of acetaldehyde, ethylene oxide and vinyl alcohol are similar, the fractional abundance of acetaldehyde is expected to be higher than that of ethylene oxide and vinyl alcohol (Bennett et al. 2005b).

4.1. Propanal and acetone

We have compared our results to predictions from the three-phase (mantle/surface/gas) astrochemical kinetics model, MAGICKAL (Model for Astrophysical Gas and Ice Chemical Kinetics And Layering), as presented in Garrod (2013). By applying a chemical network to hot-core conditions, the model follows the physico-chemical evolution of a parcel of material from the core from the free-fall collapse of the cloud to the subsequent warm-up phase of the dense core from 8 to 400 K (Garrod 2013). MAGICKAL employs a (modified) rate-equation approach to solve the coupled ice mantle, ice-surface, and gas-phase chemistry allowing radicals on the grains to meet via thermal diffusion at intermediate temperatures and form more complex molecules prior to the complete sublimation of the dust-grain ice at higher temperatures. Garrod (2013) uses three different warm-up models: *fast*, *medium* and *slow*. Here we compare our results to all three models, but note that the fast warm-up model should, in principle, be the best match to the observations because the time for this model to reach 200 K is 5×10^4 yr which is comparable to the dynamical age of $\sim 1\text{--}3 \times 10^4$ yr for IRAS16293 as derived by Schöier et al. (2002).

Garrod (2013) finds relative peak gas-phase abundances of $\text{CH}_3\text{COCH}_3 / \text{C}_2\text{H}_5\text{CHO}$ of 0.22, 0.83, and 0.07 for the fast, medium and slow model, respectively. All three models predict a higher abundance of propanal compared to acetone, which is the opposite trend of our ratio of eight. Also, the upper limit toward Sgr B2(N) reported by Belloche et al. (2013) translates into a lower limit for $\text{CH}_3\text{COCH}_3 / \text{C}_2\text{H}_5\text{CHO}$ of 3.6, which is consistent with our findings. One explanation may be that the model of Garrod (2013) uses a relatively low binding energy for acetone (3500 K), producing a desorption temperature of approx-

imately 70 K. As discussed by Garrod et al. (2008), this low-temperature desorption results in rapid destruction of acetone in the gas-phase. Our observational fit to the excitation temperature of 125 K suggests that acetone is more likely desorbed from grains at the higher temperatures more commonly associated with complex organics, which would allow the majority of grain-surface formed acetone to survive for a significant period in the gas phase.

If we compare the peak *grain-surface* abundances of acetone and propanal produced in the Garrod (2013) chemical model which would be more representative of this situation, ratios of 0.37, 2.3, and 0.39 are obtained, respectively. The quantities of acetone and propanal produced on grains in the model are, in the case of the intermediate warm-up timescale, only a factor of a few below the observed ratio. However, it should be borne in mind that the efficient production of acetone depends, in this model, on the rate at which the CH_3CO radical may be produced on the grains. This may be achieved either through direct photodissociation of CH_3CHO or by the abstraction of a H-atom from this molecule by OH or NH_2 . The rates of each of these processes are not well defined by experiment, and these uncertainties could easily induce a variation in acetone production of a few factors. It is also likely that the physical conditions, which in the Garrod (2013) model are generic, representative hot-core conditions, may not be accurate for the specific case of IRAS16293.

4.2. Ethylene oxide and acetaldehyde

Ikeda et al. (2001) searched for acetaldehyde and ethylene oxide in several massive star-forming regions. They detect both molecules in ten sources and find $\text{CH}_3\text{CHO} / \text{c-C}_2\text{H}_4\text{O}$ spanning a range from 1.2 in Sgr B2(N) to 13.2 in W51e1/e2. Belloche et al. (2013) also observed these molecules towards Sgr B2(N) and found a slightly higher value than Ikeda et al. (2001) of 3.7–7.4. It thus seems that our observed value of 12 in a low-mass YSO is toward the high end of the range observed in these high-mass regions, but that source-to-source variations may be larger than between the different groups of sources.

Occhiogrosso et al. (2014) used a two-stage (grain/gas) model, MONACO, to predict the gaseous acetaldehyde and ethylene oxide abundances during the cooling-down and subsequent warm-up phase of a hot core. At 200 K and 1.2×10^6 yrs, the fractional abundance of ethylene oxide and acetaldehyde with respect to total H is 2×10^{-9} for both molecules, which means that the relative abundance between the two species is unity. As previously mentioned, based on their laboratory experiments, Bennett et al. (2005a,b) expect the relative abundance of $\text{CH}_3\text{CHO} / \text{c-C}_2\text{H}_4\text{O}$ to be larger than unity. Again, it seems

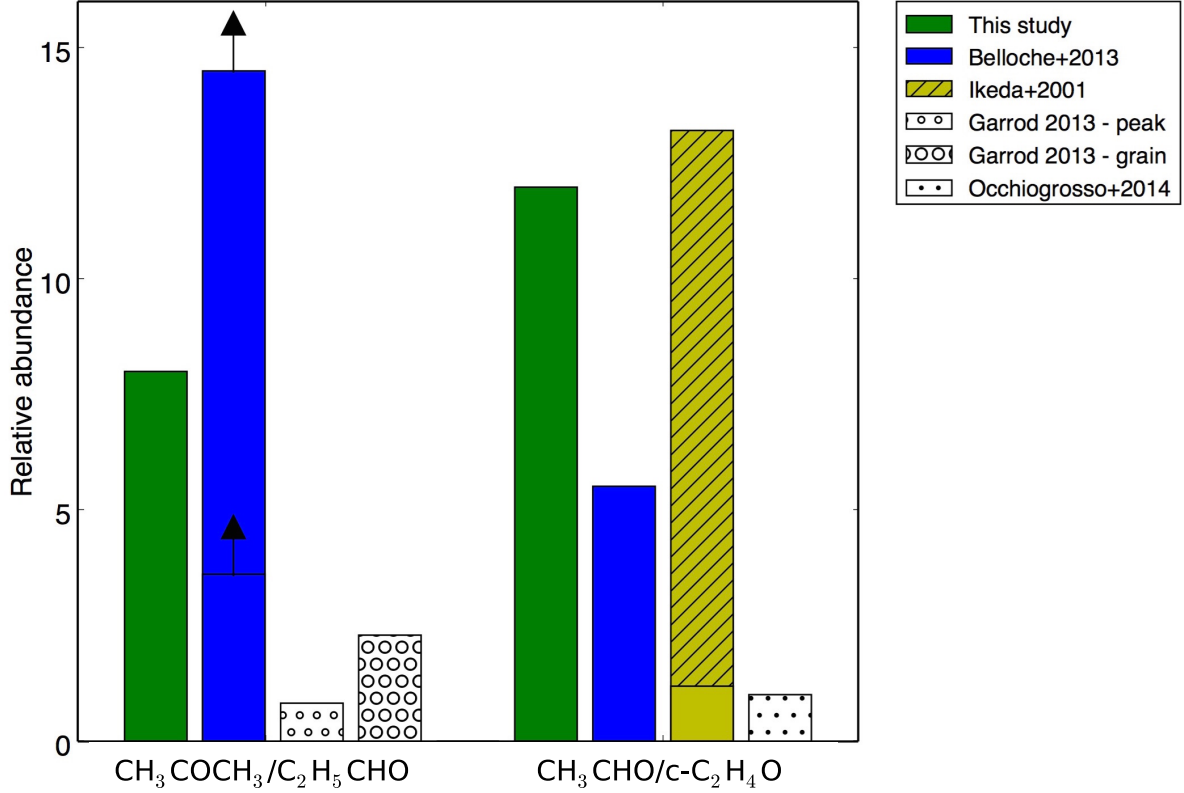


Fig. 3: Bar plot of the relative abundances of $\text{CH}_3\text{COCH}_3/\text{C}_2\text{H}_5\text{CHO}$ and $\text{CH}_3\text{CHO}/\text{c-C}_2\text{H}_4\text{O}$ from Table 1. The observations are indicated by color bars, while the chemical predictions are shown by white bars with different circle sizes. The two lower limits derived by Belloche et al. (2013) for $\text{CH}_3\text{COCH}_3/\text{C}_2\text{H}_5\text{CHO}$ are illustrated by upward arrows. The range of $\text{CH}_3\text{CHO}/\text{c-C}_2\text{H}_4\text{O}$ ratios determined in ten sources by Ikeda et al. (2001) is indicated by the hatched area. For the $\text{CH}_3\text{CHO}/\text{c-C}_2\text{H}_4\text{O}$ ratio from Belloche et al. (2013), we used the average value of the column densities of the rotational and first torsionally ($\nu_1 = 1$) excited states of acetaldehyde.

that there are some variations in the observed acetaldehyde-to-ethylene oxide ratios, and that the model results of Occhiogrosso et al. (2014) best reproduce the lower end in that range, while our measurements are at the opposite end, more than an order of magnitude above. Nevertheless, given the variations seen in the models for acetone and propanal, whether the specific physical structures of the sources can be part of the explanation remains to be explored.

5. Conclusion

We have carried out the first investigation of the oxygen bearing species in the ALMA PILS survey of the protostellar binary system IRAS16293. Our main findings are summarized as follows:

1. We have detected the molecules ethylene oxide ($\text{c-C}_2\text{H}_4\text{O}$), acetone (CH_3COCH_3), and propanal ($\text{C}_2\text{H}_5\text{CHO}$) for the first time toward a solar-type protostar. We have verified that the emission of these species, along with acetaldehyde (CH_3CHO), originates from the compact central region of the protostar, which confirms our assumption that these molecules spatially coexist. We determined a common excitation temperature, $T_{\text{ex}} \approx 125$ K for all four molecules and use this to determine column densities for each species.
2. Compared to previous observations, our results for the relative abundance ratio of $\text{CH}_3\text{COCH}_3/\text{C}_2\text{H}_5\text{CHO}$ are consistent with the lower limit found by Belloche et al. (2013) of

SgrB2(N). The ratio for $\text{CH}_3\text{CHO}/\text{c-C}_2\text{H}_4\text{O}$ is comparable to the largest value in the span of observed values of high-mass sources from Ikeda et al. (2001) (variation between the sources in that sample of approximately an order of magnitude). This suggests that the chemistry in the most central part of IRAS16293 (the hot corino region) is not significantly different from those of the high-mass hot cores, but that there may still be measurable source-to-source variations.

3. Contrary to our result, the models in Garrod (2013) predict propanal to be more abundant than acetone, except for the peak grain-surface abundances in the medium warm-up model, where the prediction is only few factors different from our result. Occhiogrosso et al. (2014) find the ratio of $\text{CH}_3\text{CHO}/\text{c-C}_2\text{H}_4\text{O}$ to be unity which is consistent with the lowest observed value of a high-mass star forming region (Ikeda et al. (2001)). All of the models investigated here return low relative abundances compared to our results, but they are however in reasonable agreement with the lowest value in the ranges reported by Ikeda et al. (2001) and Belloche et al. (2013).

The results from this paper imply that although the chemical models can reproduce the observations for some high-mass protostars reasonably well, they need to be modified to reflect the observed range of values for high-mass sources as well as our low-mass source. As discussed, the models would improve with better-defined reaction rates while including more species in the chemical networks could also improve model predictions. More

observations, in particular toward low-mass sources, are needed for comparison with models to further constrain the formation pathways.

The detections also demonstrate the great potential of spectral surveys such as PILS for identifying new species that have so far gone undetected toward solar-type stars. New detections of complex organic molecules and the determination of their relative abundances for the first time in a solar-type protostar is important because it substantiates the chemical complexity of IRAS16293 and can be used to constrain astrochemical models. The relative abundances reveal information of the formation pathway of the molecules and enable comparisons with models and laboratory experiments. In addition, the comparison of the ratios found in high-mass sources and low-mass protostars is vital to understanding the environmental effects on the formation of different molecular species.

Acknowledgements. This research was made possible through a Lundbeck Foundation Group Leader Fellowship as well as the European Research Council (ERC) under the European Union Horizon 2020 research and innovation programme (grant agreement No 646908) through ERC Consolidator Grant “S4F” to J.K.J. Research at Centre for Star and Planet Formation is funded by the Danish National Research Foundation. The work of A.C. was funded by the STFC grant ST/M001334/1. A.C. thanks the COST action CM1401 Our Astrochemical History for additional financial support. RTG acknowledges the support of the NASA APRA program, though grant NNX15AG07G. Astrochemistry in Leiden is supported by the European Union A-ERC grant 291141 CHEMPLAN, by the Netherlands Research School for Astronomy (NOVA), by a Royal Netherlands Academy of Arts and Sciences (KNAW) professor prize. The research leading to these results has received funding from the European Commission Seventh Framework Programme (FP/2007-2013) under grant agreement No 283393 (RadioNet3).

This paper makes use of the following ALMA data: ADS/JAO.ALMA#2013.1.00278.S. ALMA is a partnership of ESO (representing its member states), NSF (USA) and NINS (Japan), together with NRC (Canada) and NSC and ASIAA (Taiwan), in cooperation with the Republic of Chile. The Joint ALMA Observatory is operated by ESO, AUI/NRAO and NAOJ.

References

- Belloche, A., Müller, H. S. P., Menten, K. M., Schilke, P., & Comito, C. 2013, *A&A*, 559, A47
- Bennett, C. J., Jamieson, C. S., Osamura, Y., & Kaiser, R. I. 2005a, *ApJ*, 624, 1097
- Bennett, C. J., Osamura, Y., Lebar, M. D., & Kaiser, R. I. 2005b, *ApJ*, 634, 698
- Bisschop, S. E., Jørgensen, J. K., Bourke, T. L., Bottinelli, S., & van Dishoeck, E. F. 2008, *A&A*, 488, 959
- Blake, G. A., van Dishoeck, E. F., Jansen, D. J., Groesbeck, T. D., & Mundy, L. G. 1994, *ApJ*, 428, 680
- Bottinelli, S., Ceccarelli, C., Neri, R., et al. 2004, *ApJ*, 617, L69
- Butcher, S. S. & Wilson Jr., E. B. 1964, *J. Chem. Phys.*, 40, 1671
- Caux, E., Kahane, C., Castets, A., et al. 2011, *A&A*, 532, A23
- Cazaux, S., Tielens, A. G. G. M., Ceccarelli, C., et al. 2003, *ApJ*, 593, L51
- Ceccarelli, C. 2004, in *Astronomical Society of the Pacific Conference Series*, Vol. 323, *Star Formation in the Interstellar Medium: In Honor of David Hollenbach*, ed. D. Johnstone, F. C. Adams, D. N. C. Lin, D. A. Neufeld, & E. C. Ostriker, 195
- Ceccarelli, C., Castets, A., Caux, E., et al. 2000, *A&A*, 355, 1129
- Combes, F., Gerin, M., Wootten, A., et al. 1987, *A&A*, 180, L13
- Coutens, A., Jørgensen, J. K., van der Wiel, M. H. D., et al. 2016, *A&A*, 590, L6
- Creswell, R. A. & Schwendemann, R. H. 1974, *Chem. Phys. Lett.*, 27, 521
- Cunningham Jr., G. L., Boyd, A. W., Mayers, R. J., Gwinn, W. D., & Le Van, W. I. 1951, *J. Chem. Phys.*, 19, 676
- Demaision, J., Maes, H., van Eijck, B. P., Wlodarczak, G., & Lasne, M. C. 1987, *J. Mol. Spectrosc.*, 125, 214
- Dickens, J. E., Irvine, W. M., Ohishi, M., et al. 1997, *ApJ*, 489, 753
- Friedel, D. N. & Snyder, L. E. 2008, *ApJ*, 672, 962
- Friedel, D. N., Snyder, L. E., Remijan, A. J., & Turner, B. E. 2005, *ApJ*, 632, L95
- Fuente, A., Cernicharo, J., Caselli, P., et al. 2014, *A&A*, 568, A65
- Garrod, R. T. 2013, *ApJ*, 765, 60
- Garrod, R. T., Weaver, S. L. W., & Herbst, E. 2008, *ApJ*, 682, 283
- Goesmann, F., Rosenbauer, H., Bredehöft, J. H., et al. 2015, *Science*, 349, 020689
- Goldsmith, P. F. & Langer, W. D. 1999, *ApJ*, 517, 209
- Groner, P., Albert, S., Herbst, E., et al. 2002, *ApJS*, 142, 145
- Hardy, J. A., Cox, A. P., Fliege, E., & Dreizler, H. 1982, *Z. Naturforsch.*, 37, 1035
- Herbst, E., Giles, K., & Smith, D. 1990, *ApJ*, 358, 468
- Hirose, C. 1974, *ApJ*, 189, L145
- Hollis, J. M., Jewell, P. R., Lovas, F. J., Remijan, A., & Møllendal, H. 2004, *ApJ*, 610, L21
- Ikeda, M., Ohishi, M., Nummelin, A., et al. 2001, *ApJ*, 560, 792
- Isokoski, K., Bottinelli, S., & van Dishoeck, E. F. 2013, *A&A*, 554, A100
- Jørgensen, J. K., Bourke, T. L., Nguyen Luong, Q., & Takakuwa, S. 2011, *A&A*, 534, A100
- Jørgensen, J. K., Favre, C., Bisschop, S. E., et al. 2012, *ApJ*, 757, L4
- Jørgensen, J. K., van der Wiel, M. H. D., Coutens, A., et al. 2016, *A&A*, in press
- Kleiner, I., Lovas, F. J., & Godefroid, M. 1996, *Journal of Physical and Chemical Reference Data*, 25, 1113
- Kuan, Y., Huang, H., Charnley, S. B., et al. 2004, *ApJ*, 616, L27
- Loinard, L., Torres, R. M., Mioduszewski, A. J., & Rodríguez, L. F. 2008, *ApJ*, 675, L29
- Medcraft, C., Thompson, C. D., Robertson, E. G., Appadoo, D. R. T., & McNaughton, D. 2012, *ApJ*, 753, 18
- Müller, H. S. P., Schlöder, F., Stutzki, J., & Winnewisser, G. 2005, *Journal of Molecular Structure*, 742, 215
- Müller, H. S. P., Thorwirth, S., Roth, D. A., & Winnewisser, G. 2001, *A&A*, 370, L49
- Nummelin, A., Dickens, J. E., Bergman, P., et al. 1998, *A&A*, 337, 275
- Occhiogrosso, A., Vasyunin, A., Herbst, E., et al. 2014, *A&A*, 564, A123
- Pan, J., Albert, S., Sastry, K. V. L. N., Herbst, E., & De Lucia, F. C. 1998, *ApJ*, 499, 517
- Peng, T.-C., Despois, D., Brouillet, N., et al. 2013, *A&A*, 554, A78
- Pickett, H. M., Poynter, I. R. L., Cohen, E. A., et al. 1998, *Journal of Quantitative Spectroscopy and Radiative Transfer*, 60, 883
- Requena-Torres, M. A., Martín-Pintado, J., Martín, S., & Morris, M. R. 2008, *ApJ*, 672, 352
- Saito, S. 1976, *Chemical Physics Letters*, 42, 399
- Schöier, F. L., Jørgensen, J. K., van Dishoeck, E. F., & Blake, G. A. 2002, *A&A*, 390, 1001
- Snyder, L. E., Lovas, F. J., Mehlinger, D. M., et al. 2002, *ApJ*, 578, 245
- van Dishoeck, E. F. & Blake, G. A. 1998, *ARA&A*, 36, 317
- van Dishoeck, E. F., Blake, G. A., Jansen, D. J., & Groesbeck, T. D. 1995, *ApJ*, 447, 760

Appendix A: Observed and synthetic spectra

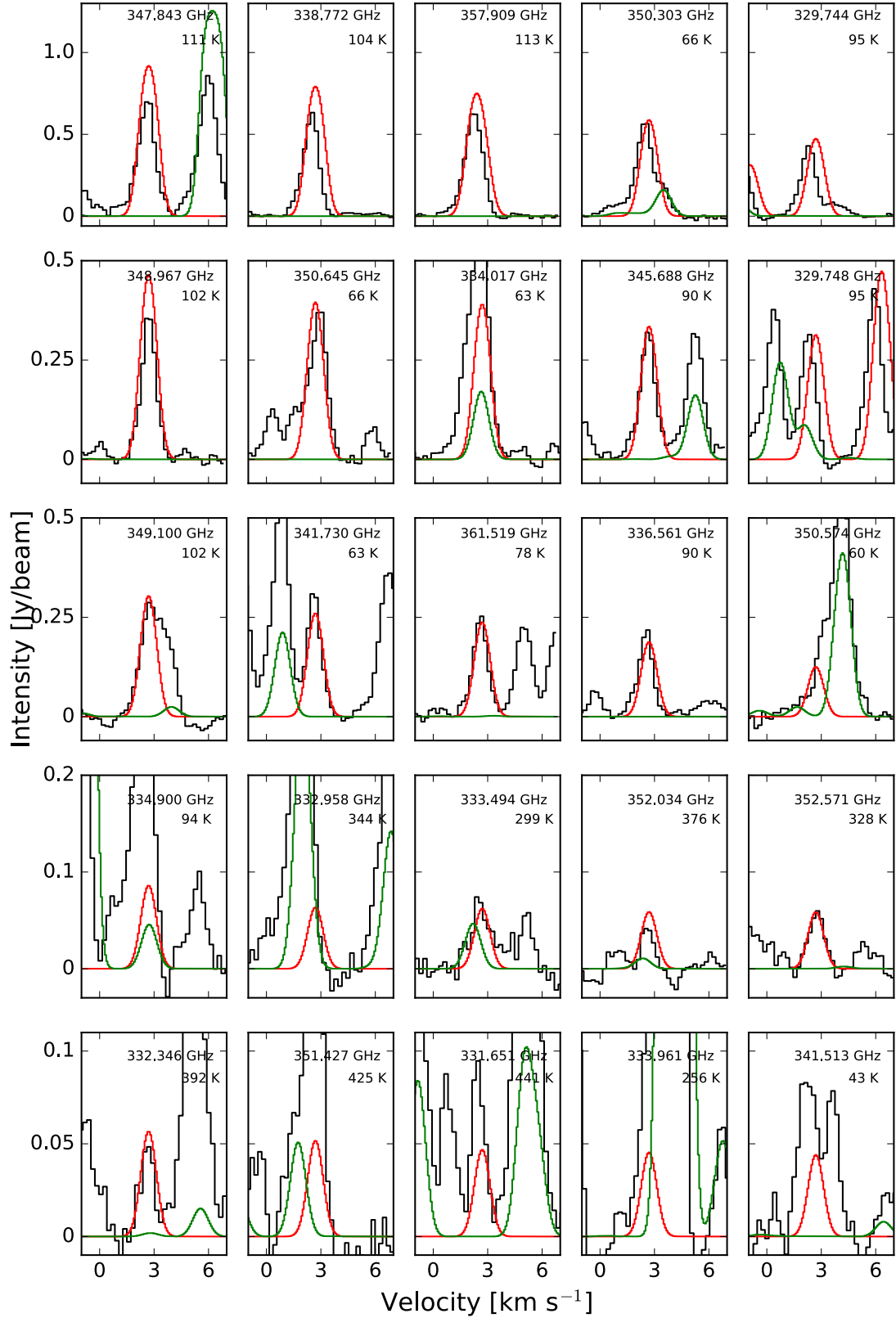


Fig. A.1: Ethylene oxide (c-C₂H₄O): Synthetic spectrum in red and reference model in green superimposed onto observed spectrum.

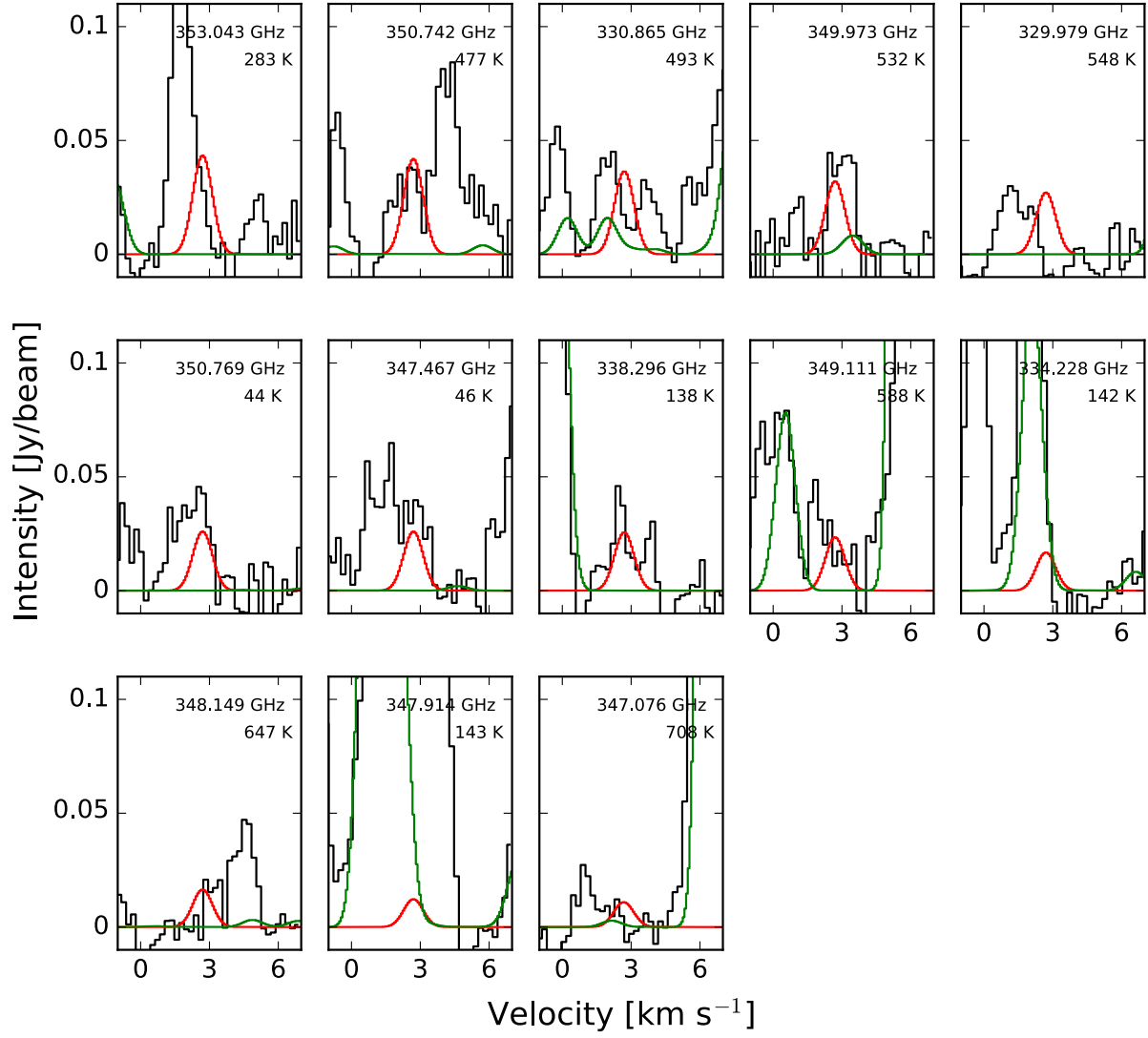


Fig. A.2: Ethylene oxide (c-C₂H₄O): Synthetic spectrum in red and reference model in green superimposed onto observed spectrum.

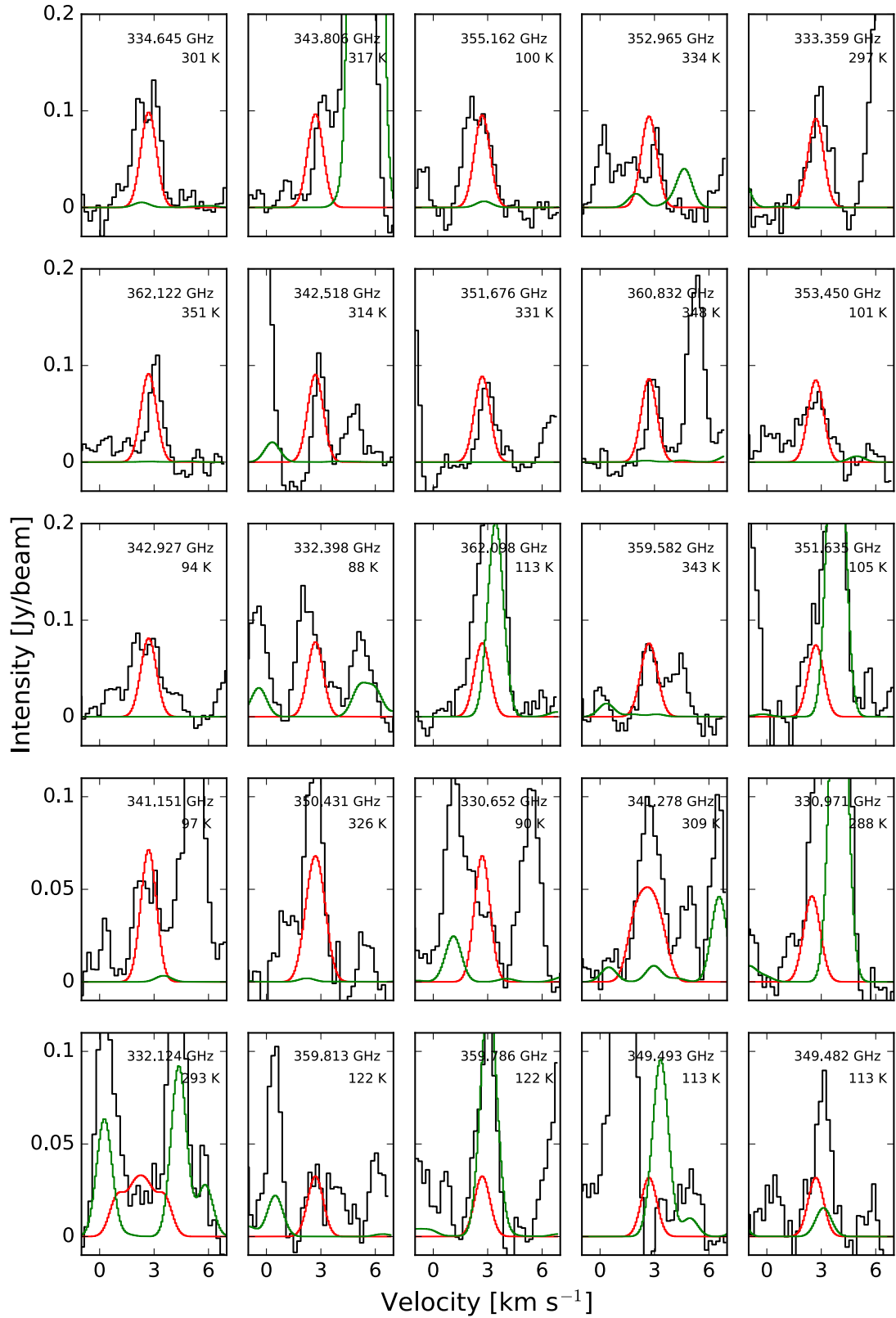


Fig. A.3: Propanal ($\text{C}_2\text{H}_5\text{CHO}$): Synthetic spectrum in red and reference model in green superimposed onto observed spectrum.

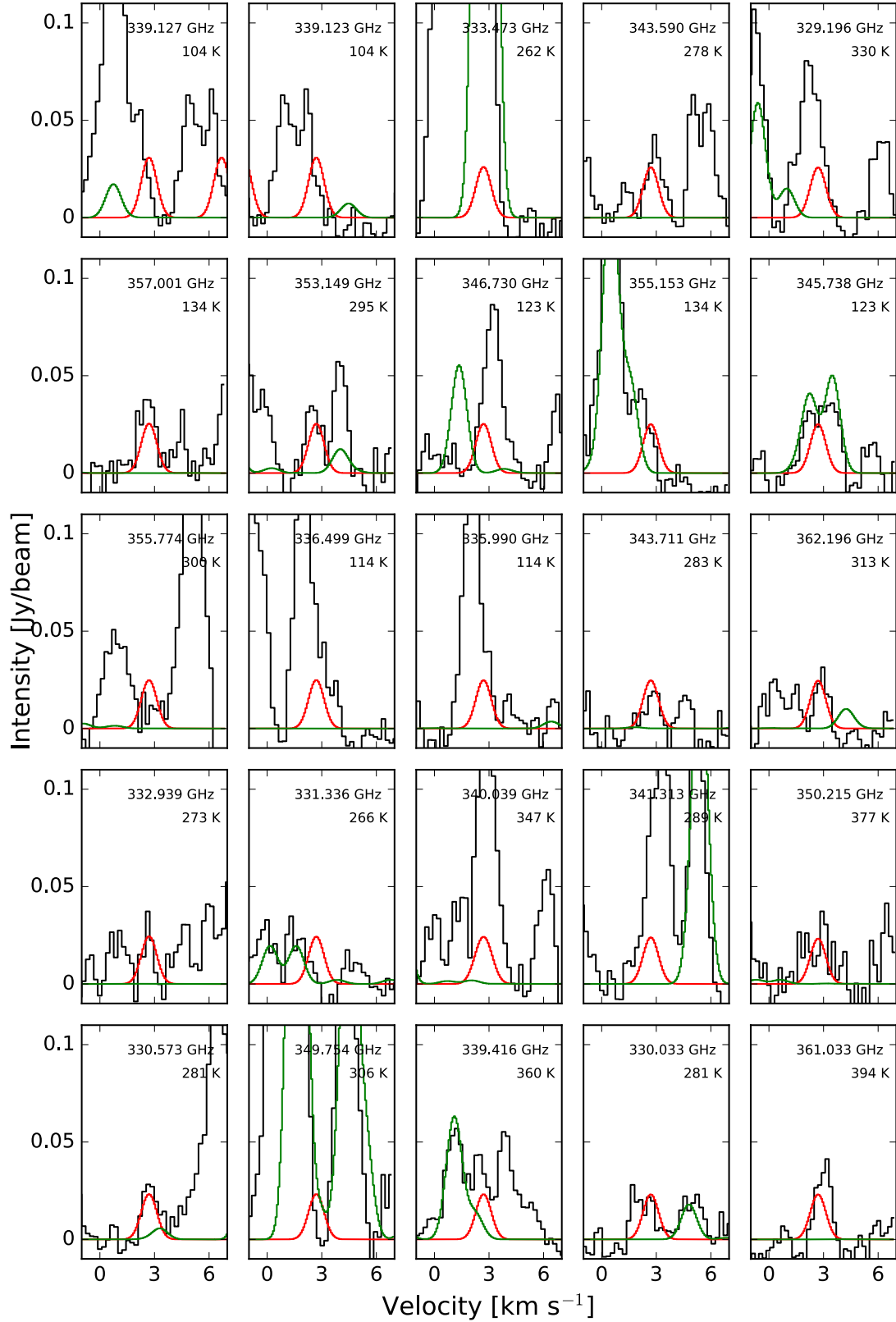


Fig. A.4: Propanal (C₂H₅CHO): Synthetic spectrum in red and reference model in green superimposed onto observed spectrum.

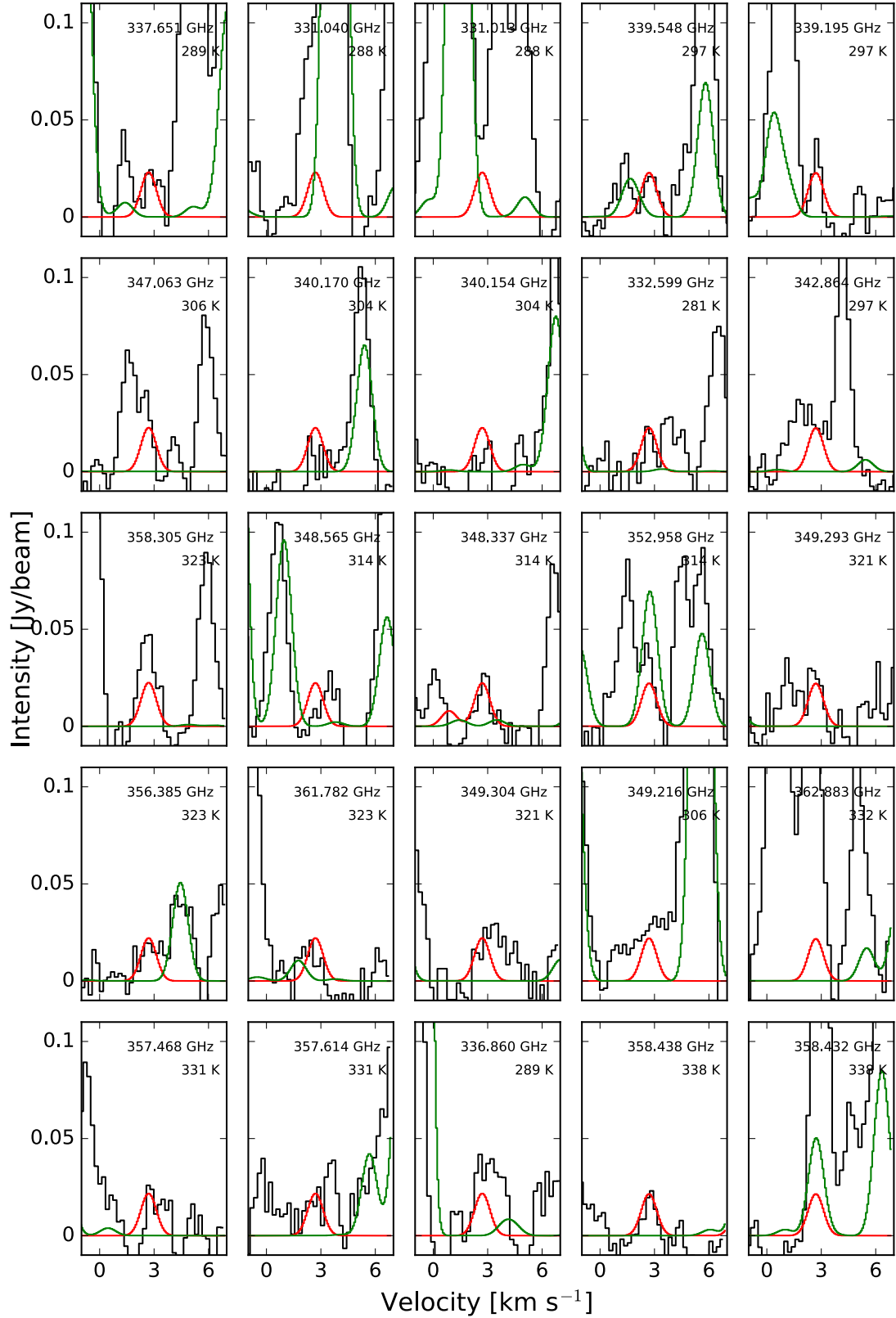


Fig. A.5: Propanal (C₂H₅CHO): Synthetic spectrum in red and reference model in green superimposed onto observed spectrum.

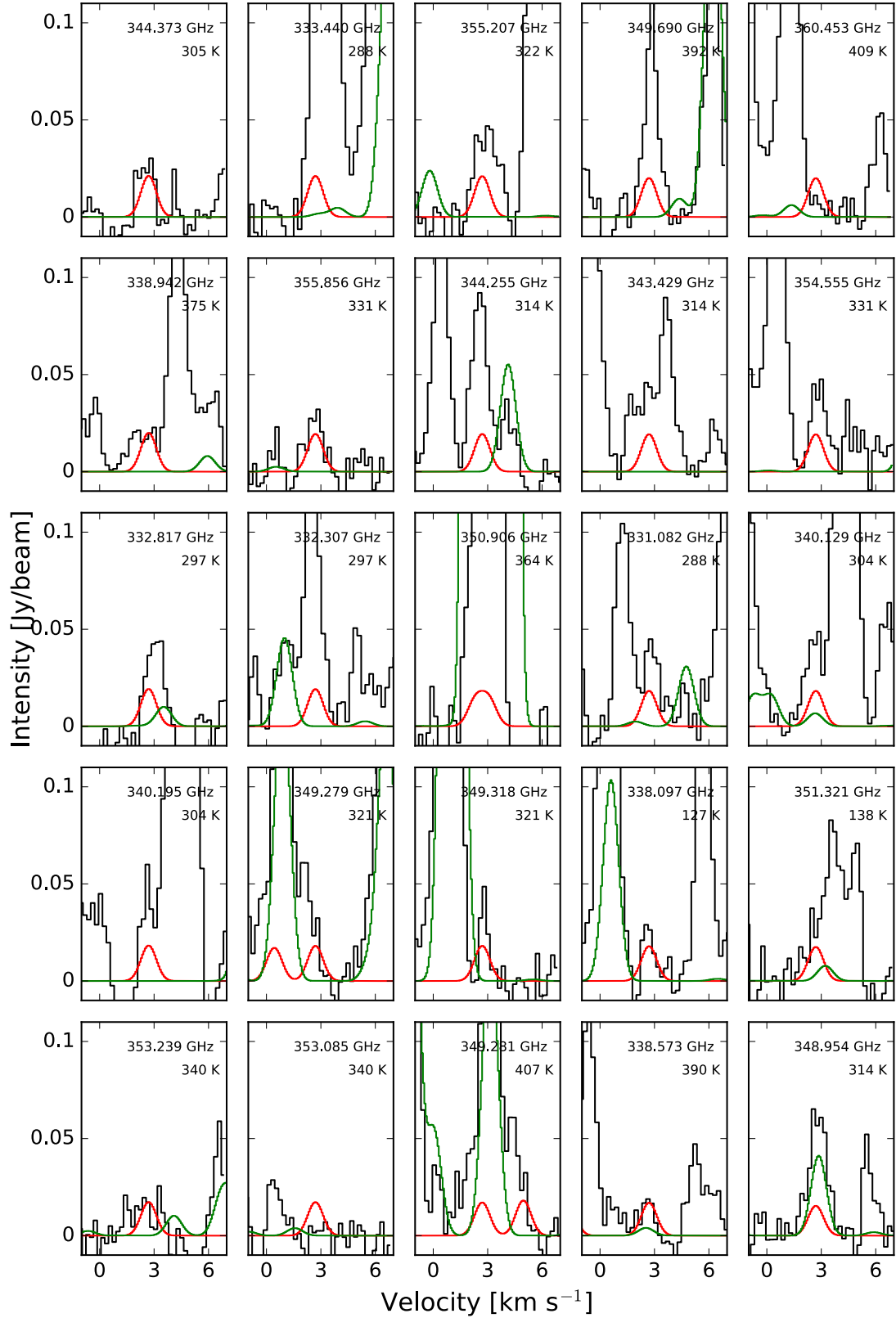


Fig. A.6: Propanal ($\text{C}_2\text{H}_5\text{CHO}$): Synthetic spectrum in red and reference model in green superimposed onto observed spectrum.

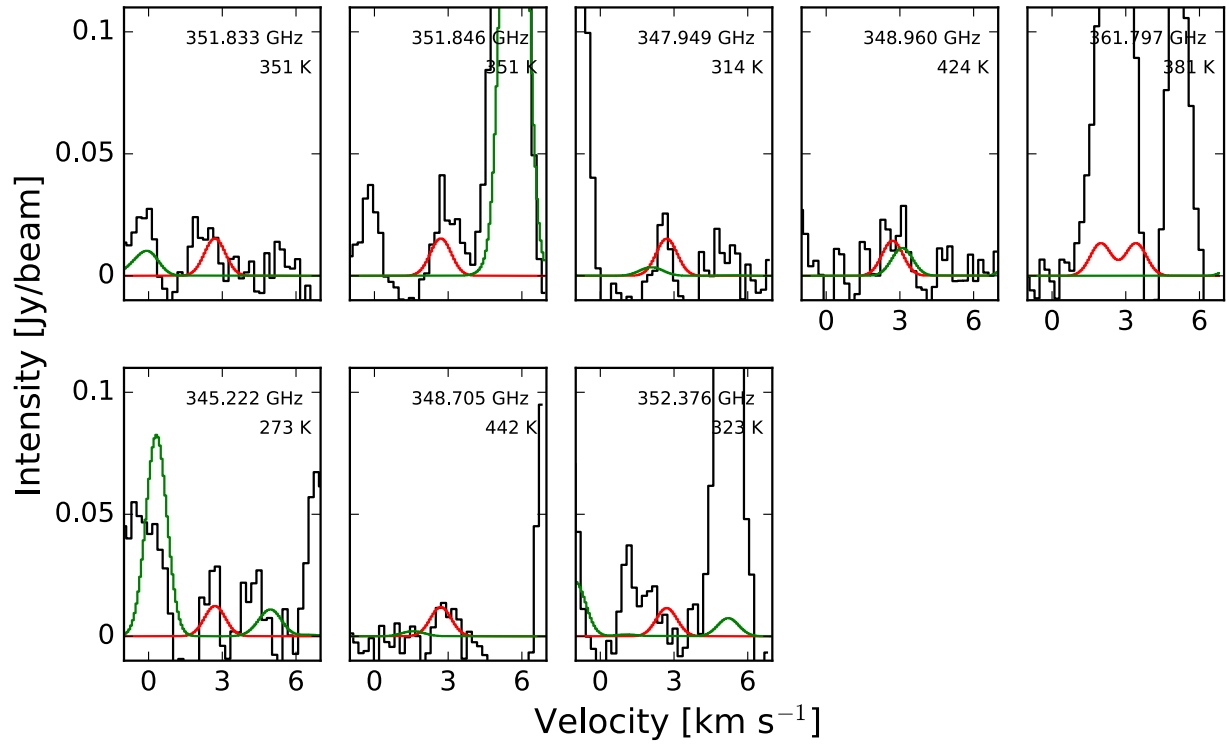


Fig. A.7: Propanal ($\text{C}_2\text{H}_5\text{CHO}$): Synthetic spectrum in red and reference model in green superimposed onto observed spectrum.

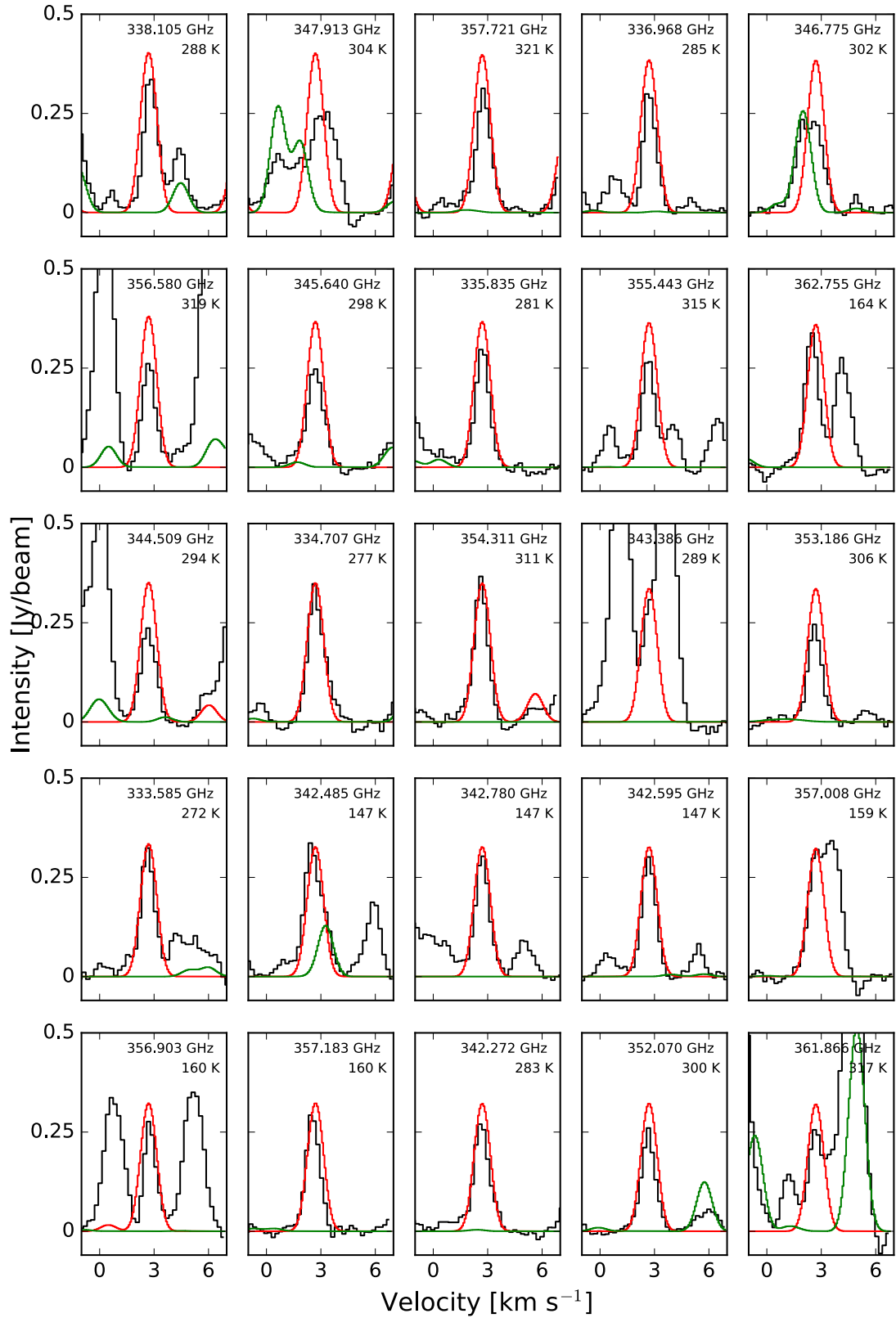


Fig. A.8: Acetone (CH₃COCH₃): Synthetic spectrum in red and reference model in green superimposed onto observed spectrum.

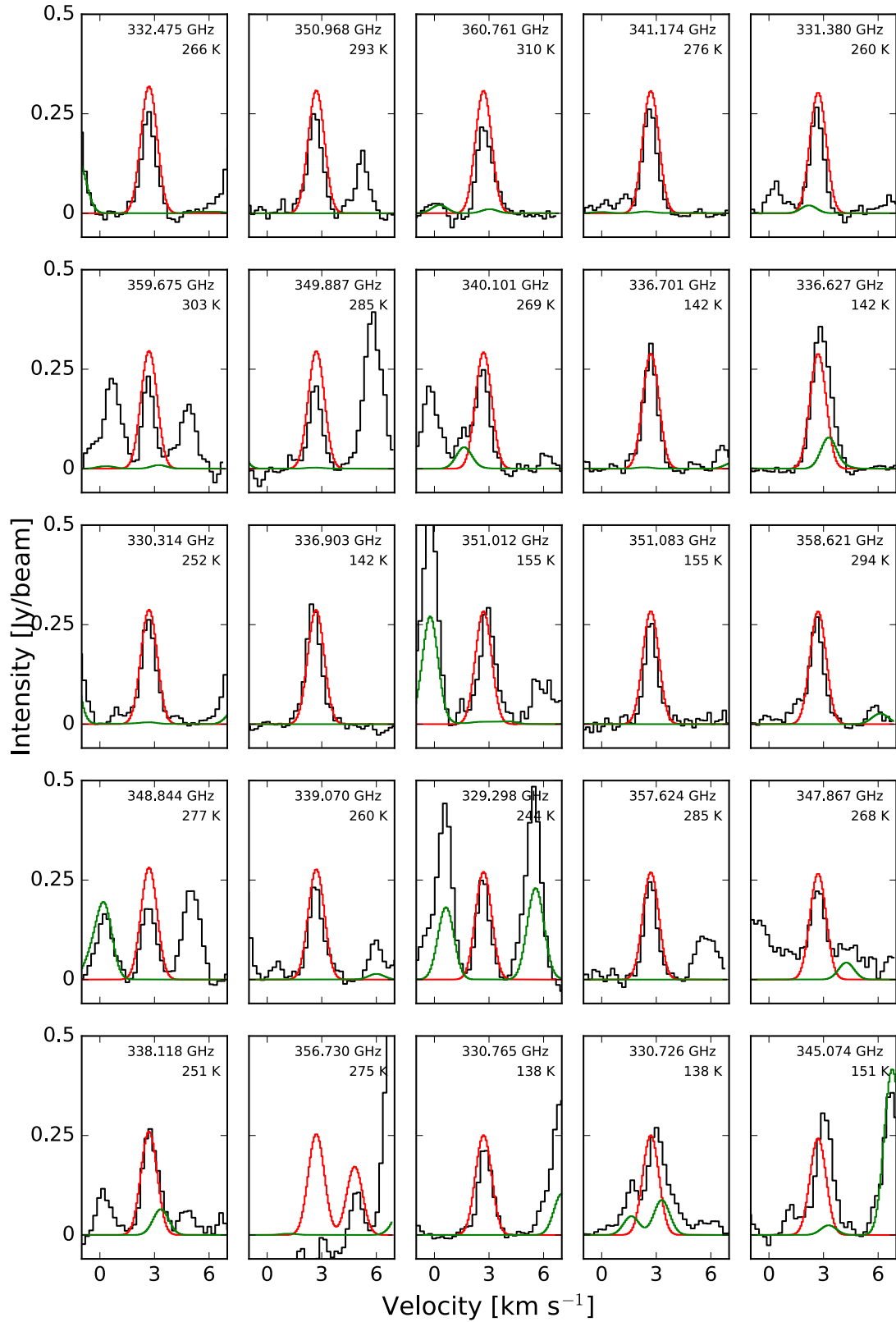


Fig. A.9: Acetone (CH₃COCH₃): Synthetic spectrum in red and reference model in green superimposed onto observed spectrum.

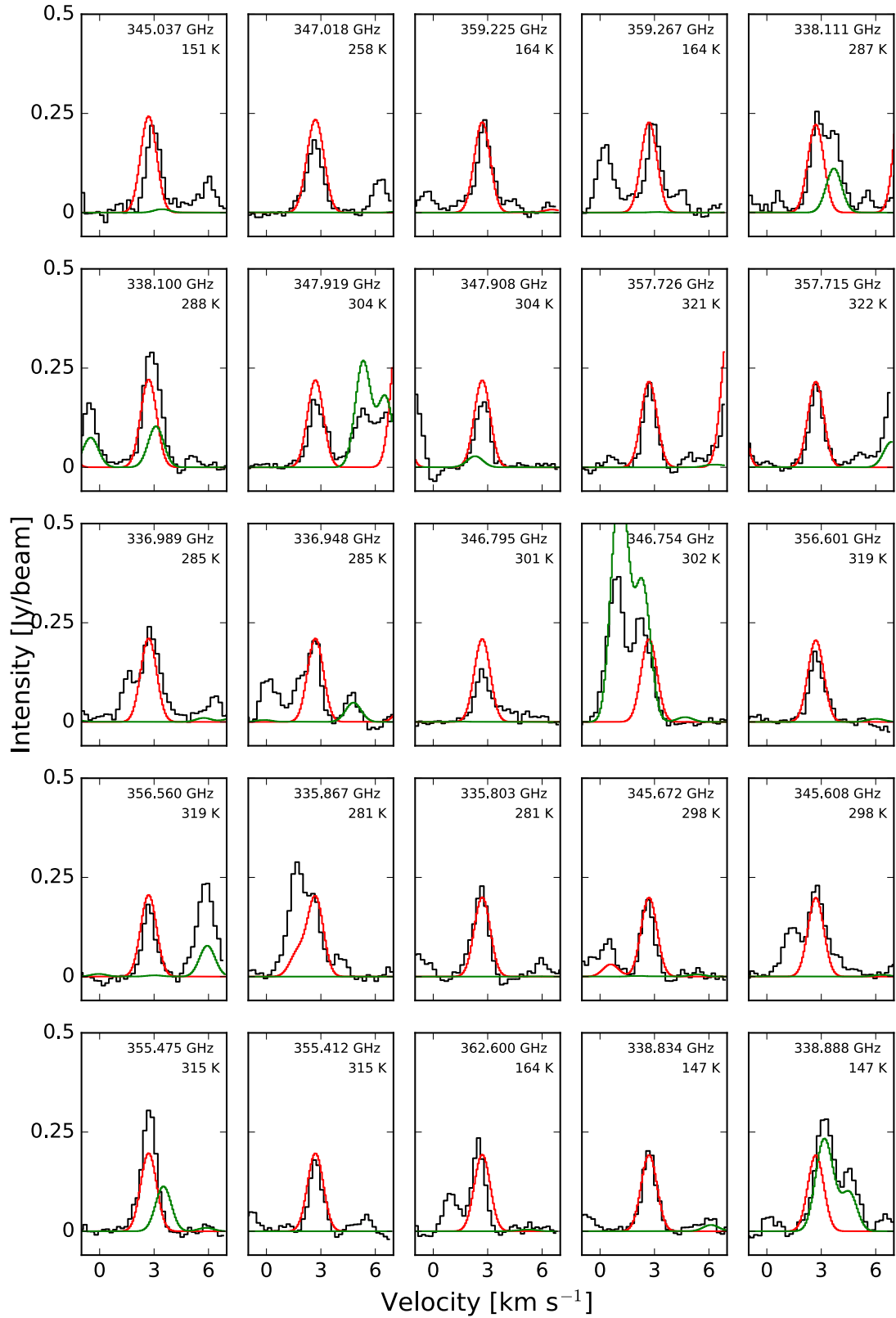


Fig. A.10: Acetone (CH_3COCH_3): Synthetic spectrum in red and reference model in green superimposed onto observed spectrum.

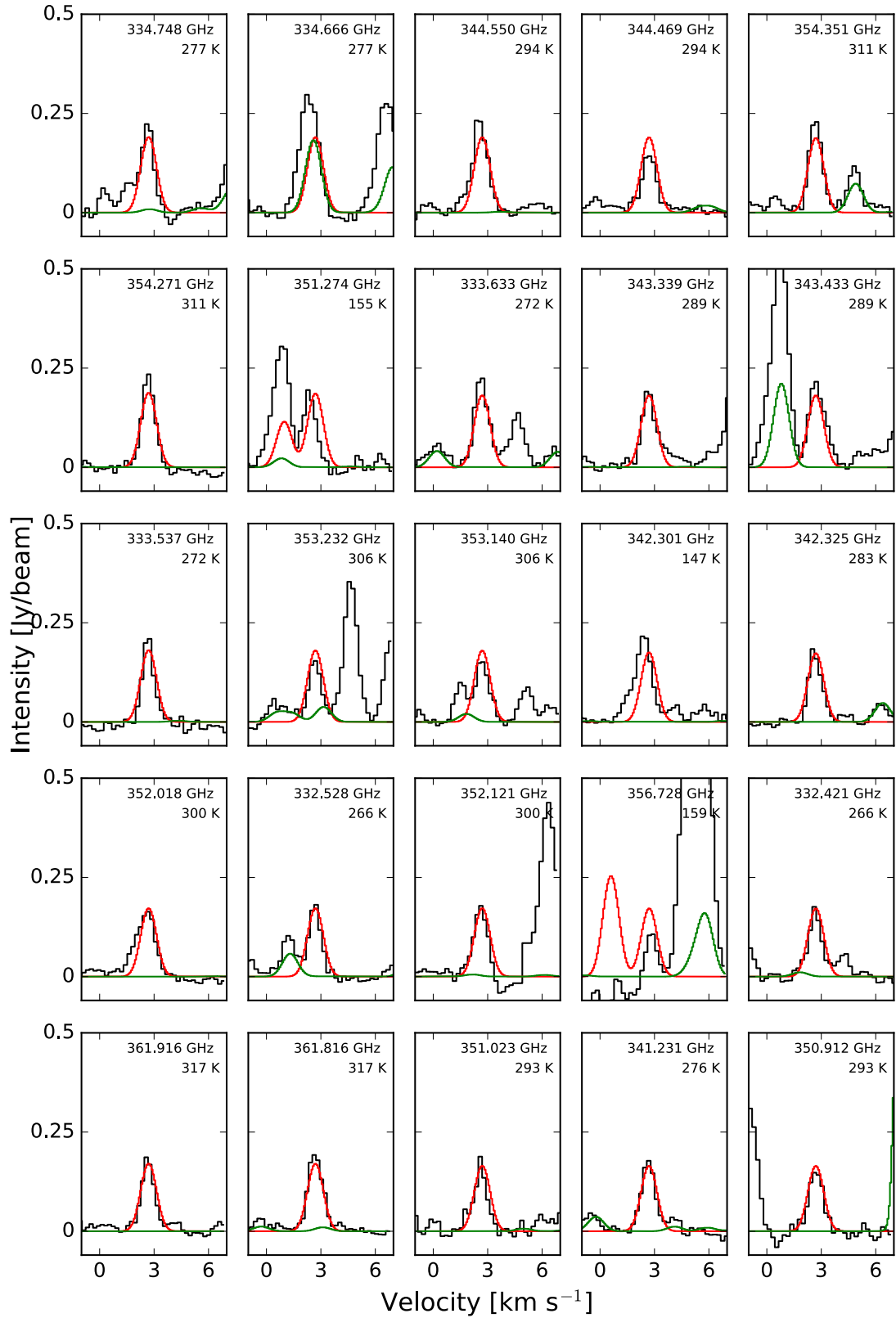


Fig. A.11: Acetone (CH_3COCH_3): Synthetic spectrum in red and reference model in green superimposed onto observed spectrum.

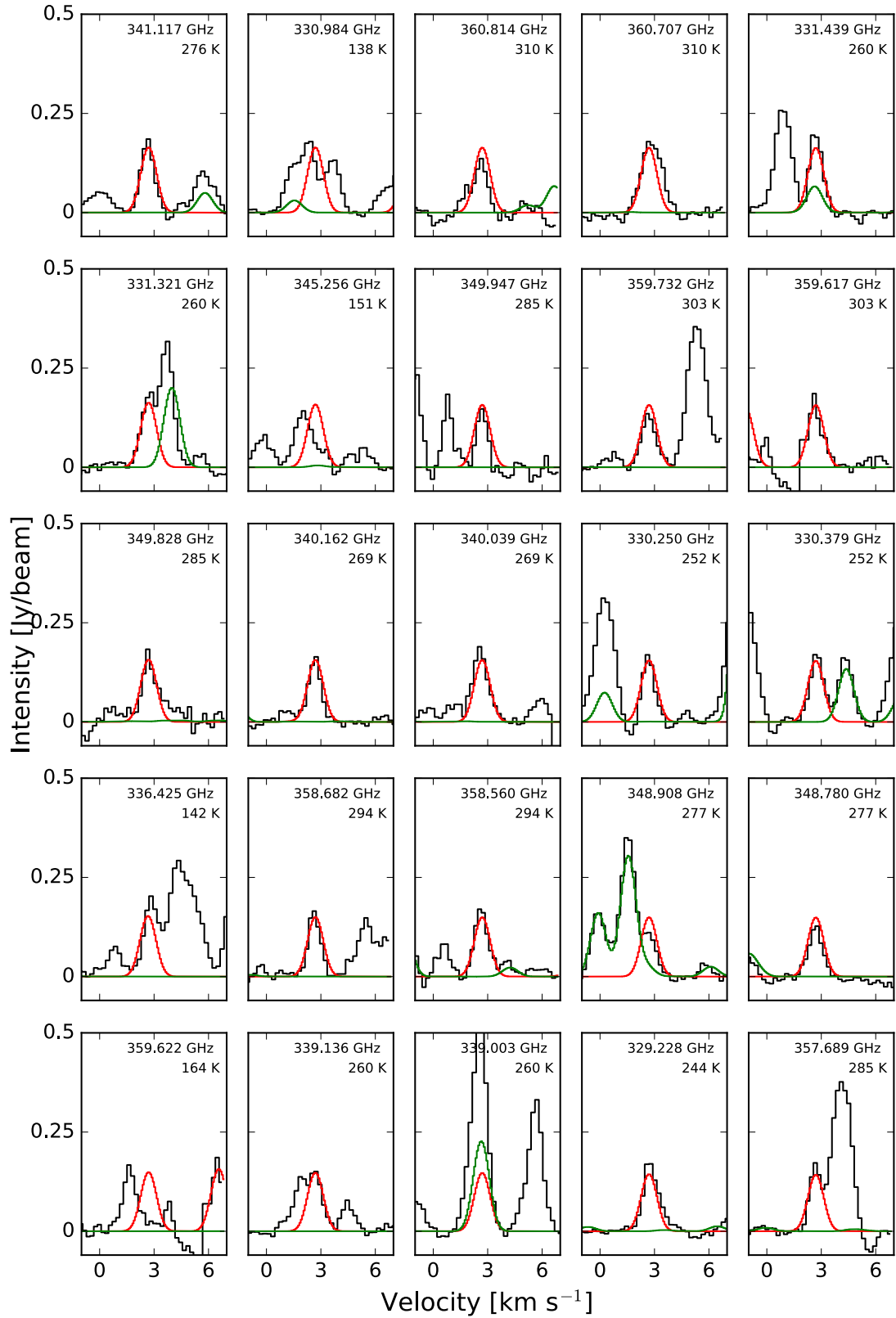


Fig. A.12: Acetone (CH_3COCH_3): Synthetic spectrum in red and reference model in green superimposed onto observed spectrum.

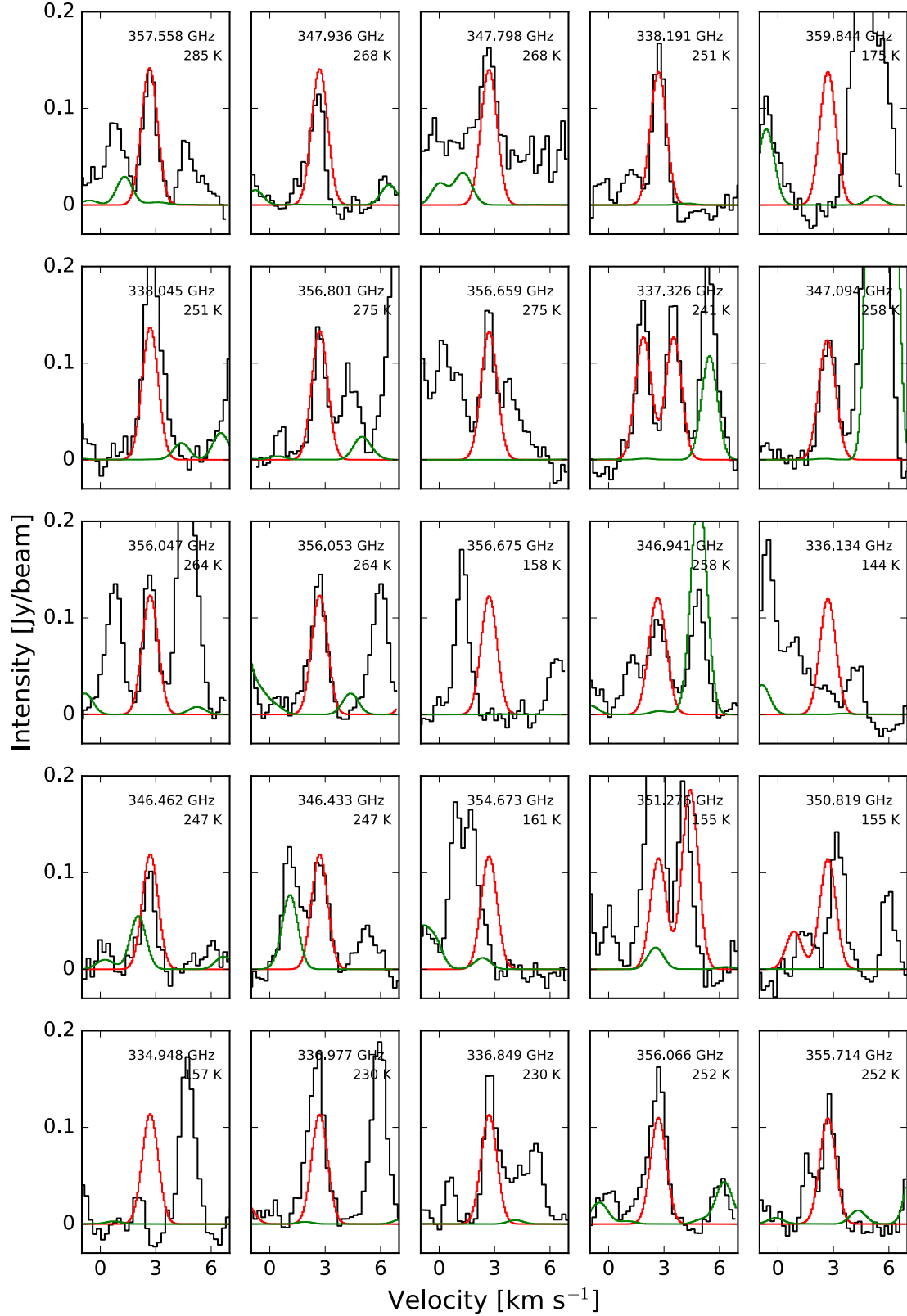


Fig. A.13: Acetone (CH_3COCH_3): Synthetic spectrum in red and reference model in green superimposed onto observed spectrum.

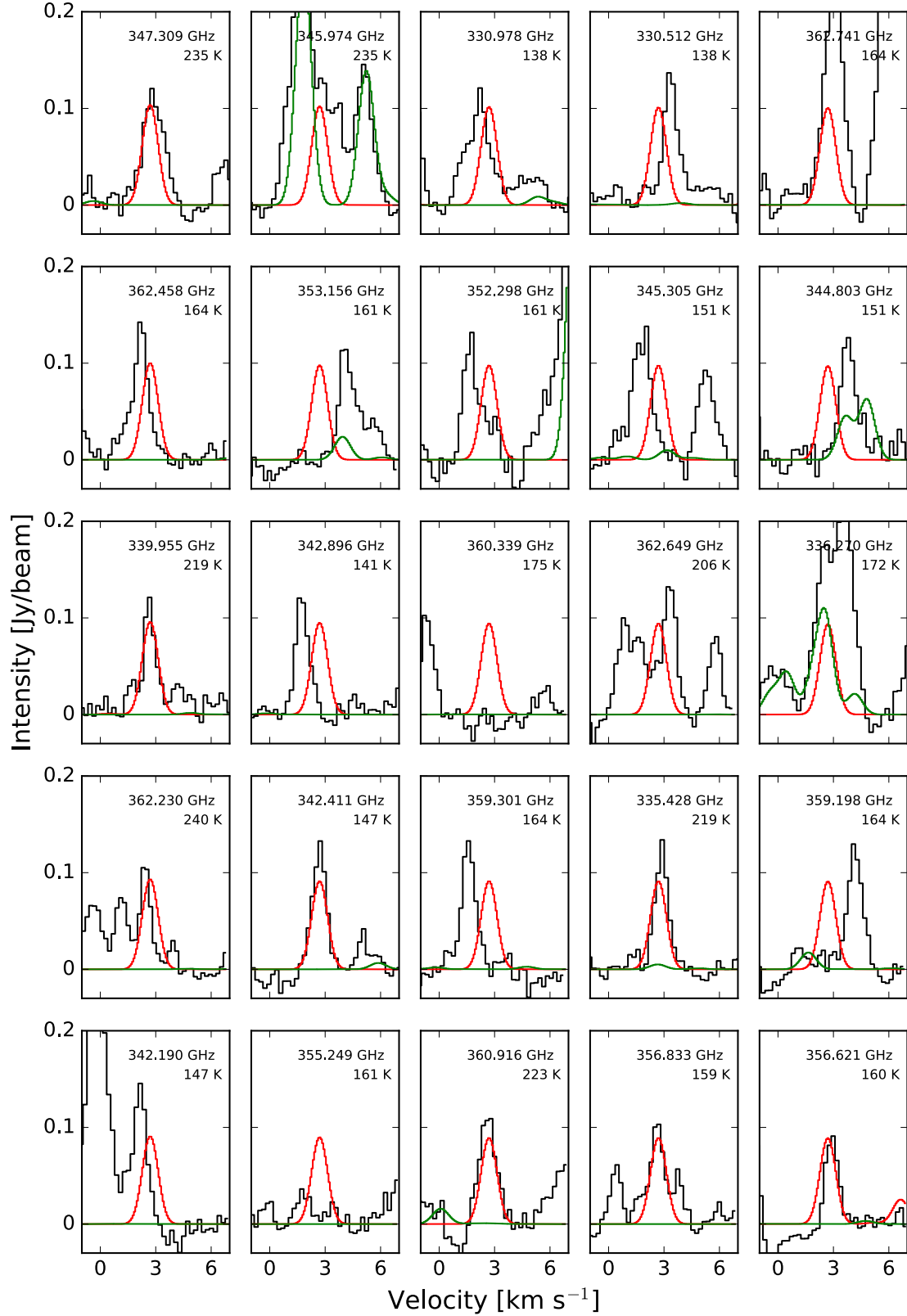


Fig. A.14: Acetone (CH_3COCH_3): Synthetic spectrum in red and reference model in green superimposed onto observed spectrum.

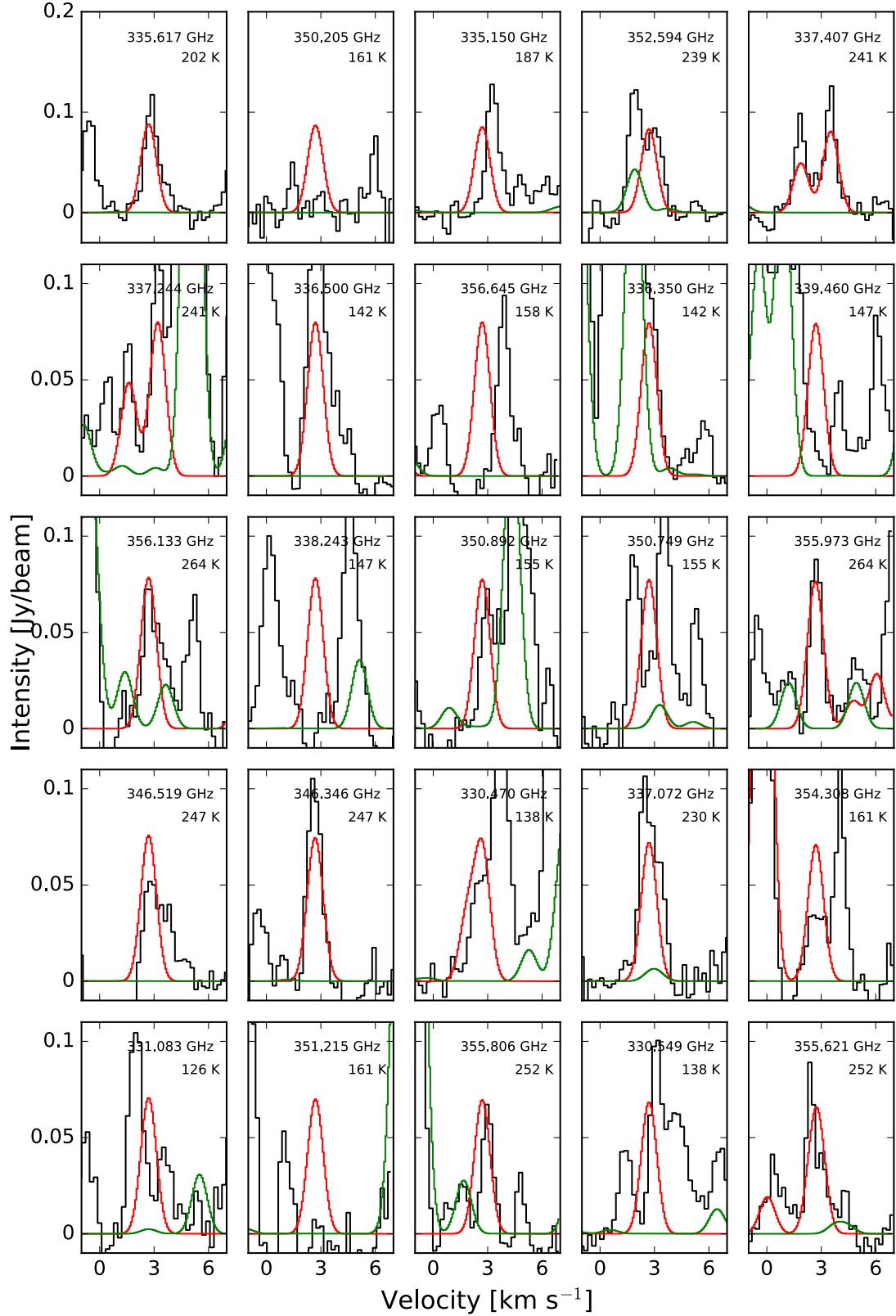


Fig. A.15: Acetone (CH_3COCH_3): Synthetic spectrum in red and reference model in green superimposed onto observed spectrum.

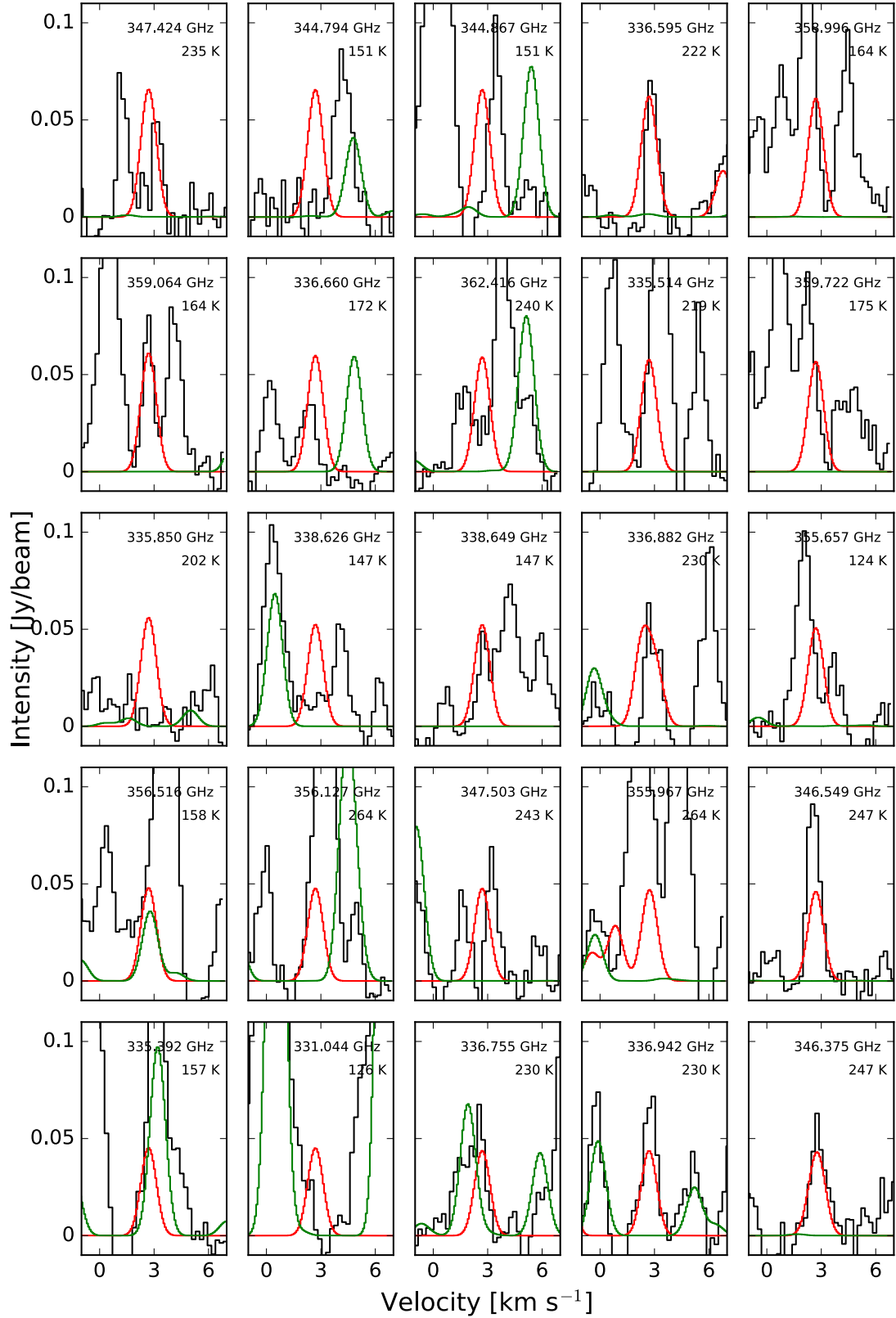


Fig. A.16: Acetone (CH_3COCH_3): Synthetic spectrum in red and reference model in green superimposed onto observed spectrum.

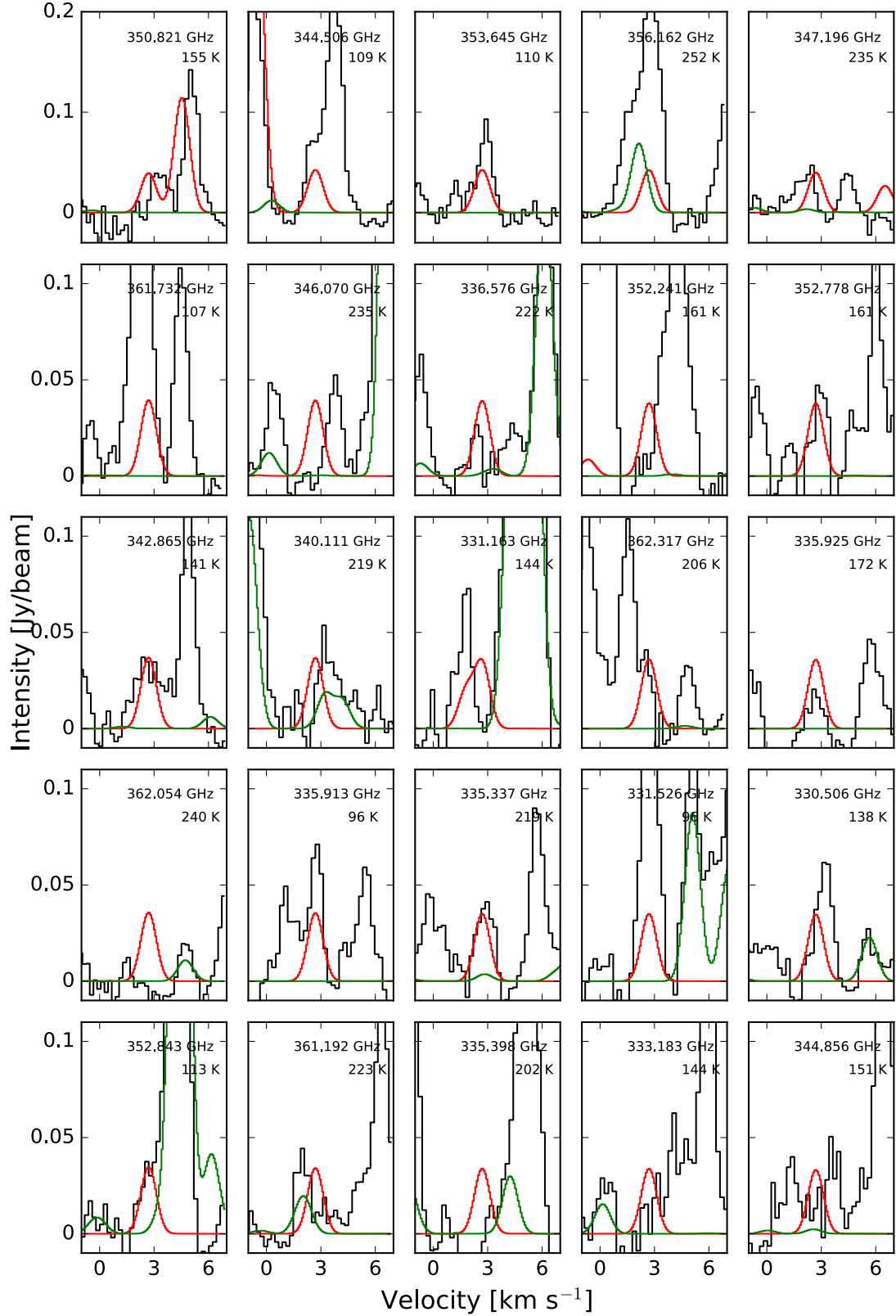


Fig. A.17: Acetone (CH_3COCH_3): Synthetic spectrum in red and reference model in green superimposed onto observed spectrum.

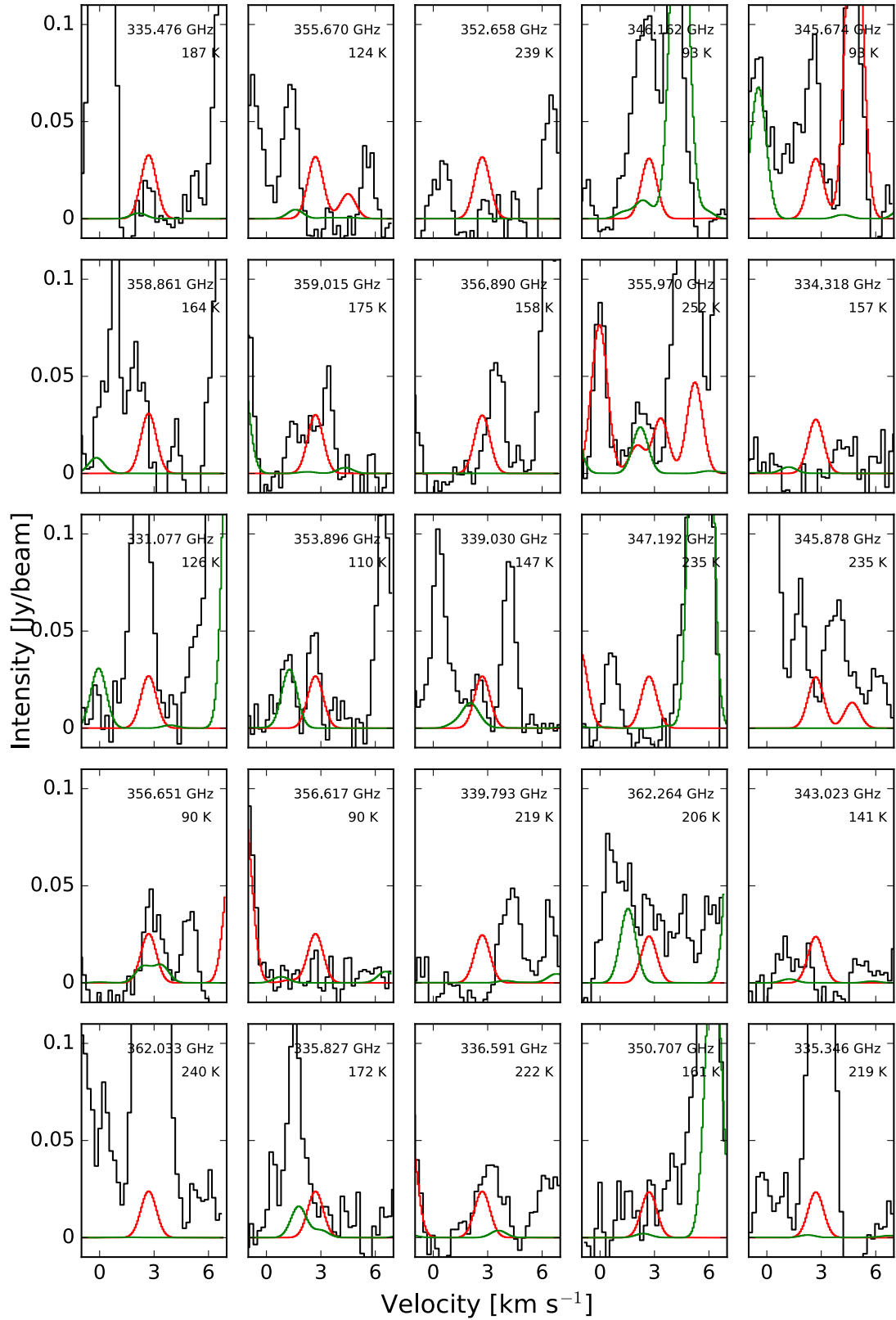


Fig. A.18: Acetone (CH_3COCH_3): Synthetic spectrum in red and reference model in green superimposed onto observed spectrum.

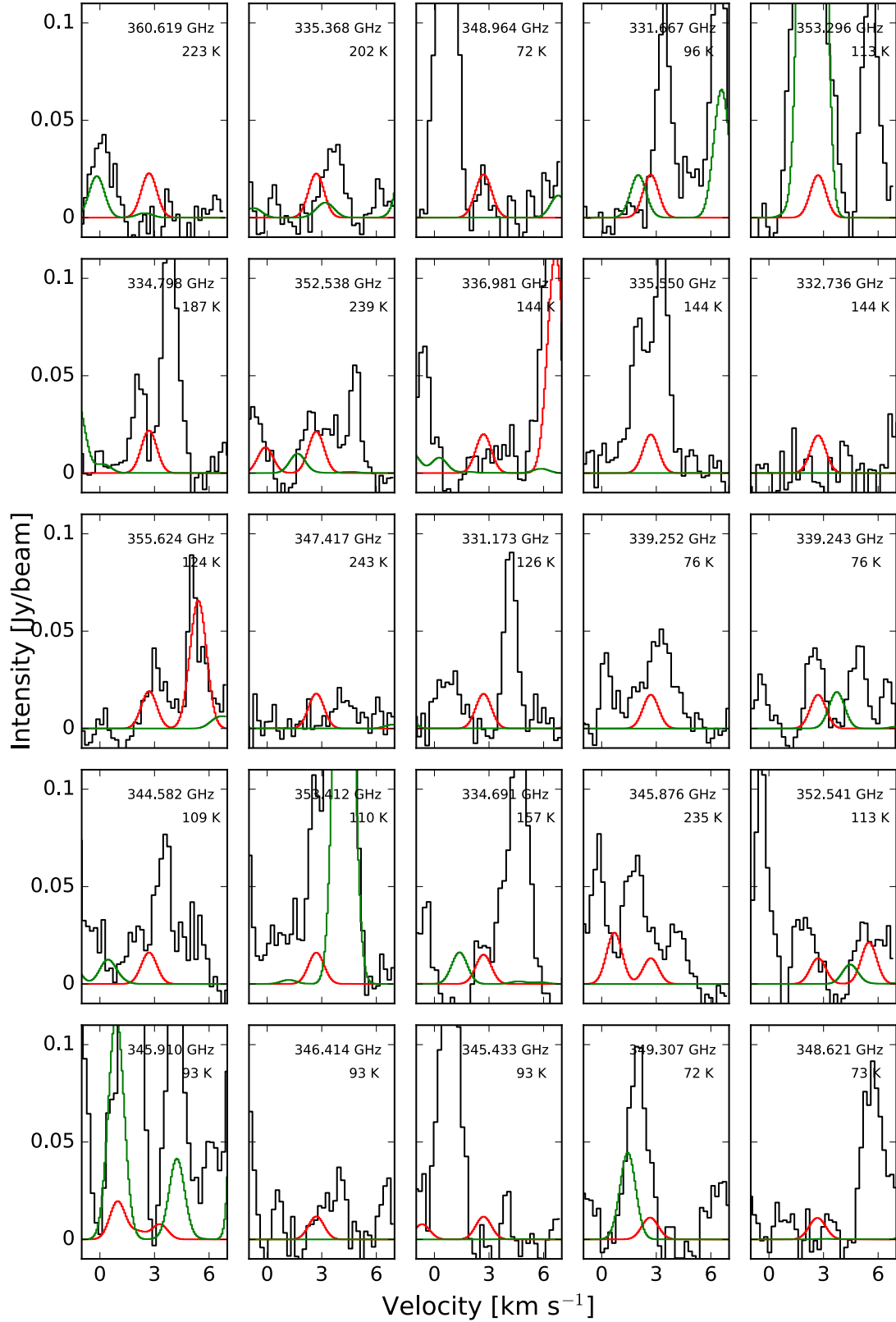


Fig. A.19: Acetone (CH_3COCH_3): Synthetic spectrum in red and reference model in green superimposed onto observed spectrum.

Appendix B: Detected lines

Table B.1: Catalog values for the detected propanal, ethylene oxide and acetone transitions and the integrated line strength of the synthetic spectrum. Due to line contamination, the integrated line strength is given for the FWHM of the Gaussian function.

Transition	Frequency [MHz]	E_{up} [K]	$\log_{10}(A_{\text{ul}})$ [s ⁻¹]	τ	$\int_{\text{FWHM}} I \delta v$ [J beam ⁻¹ km s ⁻¹]	Detection level
Ethylene oxide (c-C ₂ H ₄ O)						
10 _{2,8} – 9 _{3,7}	329744.34	95	-3.3018	5.33e-01	0.248	69
10 _{3,8} – 9 _{2,7}	329748.33	95	-3.3019	3.20e-01	0.147	41
22 _{5,17} – 22 _{4,18}	331651.32	441	-3.7416	2.58e-02	0.064	18
22 _{6,17} – 22 _{5,18}	331651.32	441	-3.7416	1.55e-02	0.064	18
21 _{4,17} – 21 _{3,18}	332345.92	392	-3.8096	1.87e-02	0.034	10
21 _{5,17} – 21 _{4,18}	332345.92	392	-3.8097	3.12e-02	0.034	10
9 _{4,5} – 8 _{5,4}	336561.39	90	-3.5297	1.71e-01	0.156	44
11 _{7,5} – 10 _{8,2}	338295.96	138	-4.5667	2.15e-02	0.027	8
11 _{1,10} – 10 _{2,9}	338771.98	104	-3.1922	4.00e-01	0.428	120
11 _{2,10} – 10 _{1,9}	338771.98	104	-3.1921	6.66e-01	0.428	120
7 _{6,1} – 6 _{5,2}	341730.22	63	-3.3675	2.38e-01	0.229	64
9 _{5,5} – 8 _{4,4}	345688.32	90	-3.4727	3.09e-01	0.249	70
12 _{0,12} – 11 _{1,11}	347843.06	111	-3.1026	7.99e-01	0.542	151
12 _{1,12} – 11 _{0,11}	347843.10	111	-3.1027	4.79e-01	0.542	151
10 _{3,7} – 9 _{4,6}	348966.62	102	-3.3039	4.50e-01	0.273	76
10 _{4,7} – 9 _{3,6}	349099.82	102	-3.3033	2.70e-01	0.246	69
24 _{6,18} – 24 _{5,19}	349972.85	532	-3.6332	1.57e-02	0.034	10
24 _{7,18} – 24 _{6,19}	349972.85	532	-3.6333	9.45e-03	0.034	10
7 _{7,1} – 6 _{6,0}	350303.48	66	-3.1488	6.08e-01	0.404	113
7 _{7,0} – 6 _{6,1}	350644.59	66	-3.1479	3.65e-01	0.291	81
23 _{5,18} – 23 _{4,19}	350741.95	477	-3.6859	1.23e-02	0.026	7
23 _{6,18} – 23 _{5,19}	350741.95	477	-3.6859	2.06e-02	0.026	7
21 _{3,18} – 21 _{2,19}	352033.68	376	-3.8513	1.73e-02	0.031	9
21 _{4,18} – 21 _{3,19}	352033.68	376	-3.8513	2.88e-02	0.031	9
20 _{2,18} – 20 _{1,19}	352570.56	328	-3.9971	2.87e-02	0.046	13
20 _{3,18} – 20 _{2,19}	352570.56	328	-3.9971	1.72e-02	0.046	13
11 _{2,9} – 10 _{3,8}	357909.16	113	-3.1776	3.47e-01	0.371	104
11 _{3,9} – 10 _{2,8}	357909.70	113	-3.1776	5.78e-01	0.531	149
8 _{6,3} – 7 _{5,2}	361519.42	78	-3.4205	1.90e-01	0.194	54
Propanal (C ₂ H ₅ CHO)						
32 _{5,28} – 31 _{5,27}	330033.48	281	-3.2366	2.04e-02	0.013	4
32 _{4,28} – 31 _{4,27}	330572.90	281	-3.2344	2.04e-02	0.022	6
13 _{9,5} – 12 _{8,4}	330651.76	90	-3.3400	3.05e-02	0.042	12
13 _{9,4} – 12 _{8,5}	330651.76	90	-3.3400	3.05e-02	0.042	12
31 _{7,25} – 30 _{7,24}	332598.70	281	-3.2339	1.96e-02	0.012	3
31 _{5,26} – 30 _{5,25}	332939.34	273	-3.2271	2.12e-02	0.019	5
35 _{1,34} – 34 _{2,33}	333358.91	297	-3.2007	2.08e-02	0.089	25
35 _{2,34} – 34 _{2,33}	333358.92	297	-3.2123	2.03e-02	0.089	25
35 _{1,34} – 34 _{1,33}	333358.93	297	-3.2123	2.03e-02	0.089	25
35 _{2,34} – 34 _{1,33}	333358.95	297	-3.2007	2.08e-02	0.089	25
32 _{6,27} – 31 _{6,26}	337650.97	289	-3.2096	1.94e-02	0.015	4
20 _{6,14} – 19 _{5,15}	338096.89	127	-3.6845	1.50e-02	0.020	5
32 _{15,17} – 31 _{15,16}	338572.87	390	-3.2943	7.07e-03	0.013	4
32 _{15,18} – 31 _{15,17}	338572.87	390	-3.2943	7.07e-03	0.013	4
33 _{5,29} – 32 _{5,28}	339194.57	297	-3.2004	1.90e-02	0.020	6
33 _{4,29} – 32 _{4,28}	339547.63	297	-3.1990	1.90e-02	0.017	5
33 _{5,29} – 32 _{4,28}	340164.32	297	-3.3742	1.27e-02	0.020	6
14 _{9,6} – 13 _{8,5}	341151.22	97	-3.3271	3.00e-02	0.052	15
14 _{9,5} – 13 _{8,6}	341151.23	97	-3.3271	3.00e-02	0.052	15
35 _{2,33} – 34 _{3,32}	341277.32	309	-3.2188	1.73e-02	0.084	23
35 _{3,33} – 34 _{3,32}	341277.92	309	-3.1853	1.87e-02	0.084	23
35 _{2,33} – 34 _{2,32}	341278.36	309	-3.1853	1.87e-02	0.084	23
35 _{3,33} – 34 _{2,32}	341278.96	309	-3.2188	1.73e-02	0.084	23

Continued on next page

Table B.1 – continued from previous page

Transition	Frequency [MHz]	E_{up} [K]	$\log_{10}(A_{\text{ul}})$ [s ⁻¹]	τ	$\int_{\text{FWHM}} I \delta v$ [J beam ⁻¹ km s ⁻¹]	Detection level
20 _{5,15} – 19 _{4,16}	341279.21	122	-3.9480	8.36e-03	0.029	8
36 _{1,35} – 35 _{2,34}	342518.47	314	-3.1633	1.94e-02	0.057	16
36 _{2,35} – 35 _{2,34}	342518.47	314	-3.1767	1.88e-02	0.057	16
36 _{1,35} – 35 _{1,34}	342518.48	314	-3.1767	1.88e-02	0.057	16
36 _{2,35} – 35 _{1,34}	342518.49	314	-3.1633	1.94e-02	0.057	16
12 _{10,2} – 11 _{9,3}	342926.51	94	-3.2160	3.40e-02	0.072	20
12 _{10,3} – 11 _{9,2}	342926.51	94	-3.2160	3.40e-02	0.072	20
31 _{6,25} – 30 _{6,24}	343589.54	278	-3.1841	2.11e-02	0.027	8
31 _{7,24} – 30 _{7,23}	343711.33	283	-3.1880	2.01e-02	0.014	4
37 _{0,37} – 36 _{1,36}	343805.93	317	-3.1164	2.15e-02	0.072	20
37 _{1,37} – 36 _{1,36}	343805.93	317	-3.1679	1.91e-02	0.072	20
37 _{0,37} – 36 _{0,36}	343805.93	317	-3.1679	1.91e-02	0.072	20
37 _{1,37} – 36 _{0,36}	343805.93	317	-3.1164	2.15e-02	0.072	20
32 _{8,25} – 31 _{8,24}	344372.65	305	-3.1927	1.71e-02	0.024	7
34 _{4,30} – 33 _{5,29}	347948.63	314	-3.3326	1.20e-02	0.011	3
34 _{5,30} – 33 _{5,29}	348337.20	314	-3.1652	1.76e-02	0.017	5
35 _{4,32} – 34 _{4,31}	349293.49	321	-3.1583	1.74e-02	0.023	6
35 _{4,32} – 34 _{3,31}	349318.44	321	-3.2457	1.42e-02	0.021	6
36 _{2,34} – 35 _{3,33}	350430.33	326	-3.1805	1.61e-02	0.111	31
36 _{3,34} – 35 _{3,33}	350430.67	326	-3.1504	1.73e-02	0.111	31
36 _{2,34} – 35 _{2,33}	350430.92	326	-3.1504	1.73e-02	0.111	31
36 _{3,34} – 35 _{2,33}	350431.26	326	-3.1805	1.61e-02	0.111	31
37 _{1,36} – 36 _{2,35}	351676.10	331	-3.1270	1.80e-02	0.050	14
37 _{2,36} – 36 _{2,35}	351676.11	331	-3.1420	1.74e-02	0.050	14
37 _{1,36} – 36 _{1,35}	351676.11	331	-3.1420	1.74e-02	0.050	14
37 _{2,36} – 36 _{1,35}	351676.11	331	-3.1270	1.80e-02	0.050	14
38 _{0,38} – 37 _{1,37}	352965.05	334	-3.0815	1.98e-02	0.047	13
38 _{1,38} – 37 _{1,37}	352965.05	334	-3.1334	1.76e-02	0.047	13
38 _{0,38} – 37 _{0,37}	352965.05	334	-3.1334	1.76e-02	0.047	13
38 _{1,38} – 37 _{0,37}	352965.05	334	-3.0815	1.98e-02	0.047	13
32 _{6,26} – 31 _{6,25}	353148.80	295	-3.1484	1.95e-02	0.029	8
13 _{10,3} – 12 _{9,4}	353450.35	101	-3.2084	3.34e-02	0.060	17
33 _{9,25} – 32 _{9,24}	354555.43	331	-3.1598	1.47e-02	0.037	10
11 _{11,0} – 10 _{10,1}	355162.35	100	-3.0902	3.74e-02	0.083	23
11 _{11,1} – 10 _{10,0}	355162.35	100	-3.0902	3.74e-02	0.083	23
33 _{9,24} – 32 _{9,23}	355856.08	331	-3.1550	1.47e-02	0.023	7
34 _{6,29} – 33 _{6,28}	356384.80	323	-3.1379	1.67e-02	0.016	5
20 _{7,13} – 19 _{6,14}	357000.67	134	-3.5090	1.92e-02	0.032	9
35 _{5,31} – 34 _{5,30}	357467.93	331	-3.1310	1.63e-02	0.012	3
35 _{4,31} – 34 _{4,30}	357613.69	331	-3.1304	1.63e-02	0.016	5
34 _{5,29} – 33 _{5,28}	358305.47	323	-3.1306	1.68e-02	0.037	10
36 _{3,33} – 35 _{3,32}	358438.34	338	-3.1242	1.60e-02	0.015	4
37 _{2,35} – 36 _{3,34}	359581.63	343	-3.1434	1.50e-02	0.060	17
37 _{3,35} – 36 _{3,34}	359581.82	343	-3.1164	1.59e-02	0.060	17
37 _{2,35} – 36 _{2,34}	359581.97	343	-3.1164	1.59e-02	0.060	17
37 _{3,35} – 36 _{2,34}	359582.16	343	-3.1434	1.50e-02	0.060	17
18 _{8,10} – 17 _{7,11}	359812.79	122	-3.3969	2.43e-02	0.030	8
38 _{1,37} – 37 _{2,36}	360831.75	348	-3.0917	1.66e-02	0.059	16
38 _{2,37} – 37 _{2,36}	360831.75	348	-3.1082	1.60e-02	0.059	16
38 _{1,37} – 37 _{1,36}	360831.75	348	-3.1082	1.60e-02	0.059	16
38 _{2,37} – 37 _{1,36}	360831.75	348	-3.0917	1.66e-02	0.059	16
34 _{13,22} – 33 _{13,21}	361033.21	394	-3.1711	8.54e-03	0.028	8
34 _{13,21} – 33 _{13,20}	361033.31	394	-3.1711	8.54e-03	0.028	8
39 _{0,39} – 38 _{1,38}	362122.12	351	-3.0475	1.82e-02	0.067	19
39 _{0,39} – 38 _{0,38}	362122.12	351	-3.0999	1.61e-02	0.067	19
39 _{1,39} – 38 _{0,38}	362122.12	351	-3.0475	1.82e-02	0.067	19
39 _{1,39} – 38 _{1,38}	362122.12	351	-3.0999	1.61e-02	0.067	19
33 _{6,27} – 32 _{6,26}	362196.30	313	-3.1159	1.80e-02	0.019	5

Continued on next page

Table B.1 – continued from previous page

Transition	Frequency [MHz]	E_{up} [K]	$\log_{10}(A_{\text{ul}})$ [s ⁻¹]	τ	$\int_{\text{FWHM}} I \delta v$ [J beam ⁻¹ km s ⁻¹]	Detection level
Acetone (CH ₃ COCH ₃)						
26 _{8,18} – 25 _{9,17} EA	329228.06	244	-2.9657	3.38e-02	0.130	36
26 _{9,18} – 25 _{8,17} EA	329228.06	244	-2.9657	3.38e-02	0.130	36
26 _{8,18} – 25 _{9,17} AE	329228.14	244	-2.9657	1.69e-02	0.130	36
26 _{9,18} – 25 _{8,17} AE	329228.14	244	-2.9657	5.07e-02	0.130	36
26 _{8,18} – 25 _{9,17} EE	329298.16	244	-2.9656	1.35e-01	0.178	50
26 _{9,18} – 25 _{8,17} EE	329298.16	244	-2.9656	1.35e-01	0.178	50
14 _{7,8} – 13 _{4,9} AA	329367.94	80	-4.0975	1.27e-02	0.118	33
26 _{8,18} – 25 _{9,17} AA	329368.09	244	-2.9654	5.07e-02	0.117	33
26 _{9,18} – 25 _{8,17} AA	329368.10	244	-2.9654	8.45e-02	0.117	33
27 _{7,20} – 26 _{8,19} EA	330250.07	252	-2.9233	3.60e-02	0.114	32
27 _{8,20} – 26 _{7,19} EA	330250.07	252	-2.9233	3.60e-02	0.114	32
27 _{7,20} – 26 _{8,19} AE	330250.13	252	-2.9233	5.40e-02	0.114	32
27 _{8,20} – 26 _{7,19} AE	330250.13	252	-2.9232	1.80e-02	0.114	32
51 _{13,38} – 51 _{13,39} EE	330250.15	875	-3.5999	2.36e-04	0.114	32
51 _{14,38} – 51 _{13,39} EE	330250.15	875	-3.2461	5.32e-04	0.114	32
51 _{13,38} – 51 _{12,39} EE	330250.15	875	-3.2461	5.32e-04	0.114	32
51 _{14,38} – 51 _{12,39} EE	330250.15	875	-3.5999	2.36e-04	0.114	32
27 _{7,20} – 26 _{8,19} EE	330314.39	252	-2.9231	1.44e-01	0.198	55
27 _{8,20} – 26 _{7,19} EE	330314.39	252	-2.9231	1.44e-01	0.198	55
27 _{7,20} – 26 _{8,19} AA	330378.56	252	-2.9230	9.00e-02	0.122	34
27 _{8,20} – 26 _{7,19} AA	330378.56	252	-2.9230	5.40e-02	0.122	34
17 _{15,3} – 16 _{14,2} AE	330506.31	138	-2.8918	3.06e-02	0.035	10
17 _{15,2} – 16 _{14,3} AE	330512.29	138	-2.8918	9.19e-02	0.038	11
17 _{15,3} – 16 _{14,3} EA	330549.33	138	-2.8919	6.13e-02	0.057	16
17 _{15,2} – 16 _{14,2} EE	330725.88	138	-2.8905	2.45e-01	0.207	58
17 _{15,3} – 16 _{14,3} EE	330765.02	138	-2.8906	2.45e-01	0.153	43
13 _{3,10} – 12 _{2,11} EE	331129.66	60	-4.7227	5.19e-03	0.015	4
13 _{4,10} – 12 _{1,11} EE	331129.71	60	-4.7227	5.19e-03	0.015	4
28 _{6,22} – 27 _{7,21} EA	331321.41	260	-2.8862	3.80e-02	0.148	41
28 _{7,22} – 27 _{6,21} EA	331321.41	260	-2.8862	3.80e-02	0.148	41
28 _{6,22} – 27 _{7,21} AE	331321.46	260	-2.8863	1.90e-02	0.148	41
28 _{7,22} – 27 _{6,21} AE	331321.46	260	-2.8863	5.70e-02	0.148	41
28 _{7,22} – 27 _{7,21} EE	331380.50	260	-3.0073	1.15e-01	0.191	53
28 _{6,22} – 27 _{7,21} EE	331380.50	260	-3.4997	3.70e-02	0.191	53
28 _{6,22} – 27 _{6,21} EE	331380.50	260	-3.0094	1.15e-01	0.191	53
28 _{7,22} – 27 _{6,21} EE	331380.50	260	-3.4932	3.76e-02	0.191	53
29 _{5,24} – 28 _{5,23} EA	332420.74	266	-2.8535	4.00e-02	0.116	33
29 _{6,24} – 28 _{6,23} EA	332420.74	266	-2.8535	4.00e-02	0.116	33
29 _{5,24} – 28 _{5,23} AE	332420.79	266	-2.8535	2.00e-02	0.116	33
29 _{6,24} – 28 _{6,23} AE	332420.79	266	-2.8535	6.00e-02	0.116	33
29 _{5,24} – 28 _{5,23} EE	332474.57	266	-3.4029	4.52e-02	0.185	52
29 _{5,24} – 28 _{6,23} EE	332474.57	266	-2.9972	1.15e-01	0.185	52
29 _{6,24} – 28 _{6,23} EE	332474.57	266	-3.4029	4.52e-02	0.185	52
29 _{6,24} – 28 _{5,23} EE	332474.57	266	-2.9972	1.15e-01	0.185	52
29 _{6,24} – 28 _{6,23} AA	332528.32	266	-2.8532	1.00e-01	0.125	35
29 _{5,24} – 28 _{5,23} AA	332528.32	266	-2.8532	6.00e-02	0.125	35
30 _{4,26} – 29 _{5,25} EA	333537.35	272	-2.8239	4.20e-02	0.139	39
30 _{5,26} – 29 _{4,25} EA	333537.35	272	-2.8239	4.20e-02	0.139	39
30 _{5,26} – 29 _{5,25} AE	333537.39	272	-2.8240	2.10e-02	0.139	39
30 _{4,26} – 29 _{4,25} AE	333537.39	272	-2.8240	6.30e-02	0.139	39
30 _{4,26} – 29 _{4,25} EE	333585.34	272	-4.7355	2.06e-03	0.235	66
30 _{5,26} – 29 _{4,25} EE	333585.34	272	-2.8291	1.66e-01	0.235	66
30 _{4,26} – 29 _{5,25} EE	333585.34	272	-2.8291	1.66e-01	0.235	66
30 _{5,26} – 29 _{5,25} EE	333585.34	272	-4.7355	2.06e-03	0.235	66
30 _{4,26} – 29 _{5,25} AA	333633.28	272	-2.8236	6.30e-02	0.170	48
30 _{5,26} – 29 _{4,25} AA	333633.28	272	-2.8237	1.05e-01	0.170	48
19 _{13,7} – 18 _{12,6} AE	334691.41	157	-3.2379	1.29e-02	0.018	5
31 _{3,28} – 30 _{3,27} EE	334706.67	277	-3.2332	6.39e-02	0.255	71

Continued on next page

Table B.1 – continued from previous page

Transition	Frequency [MHz]	E_{up} [K]	$\log_{10}(A_{\text{ul}})$ [s ⁻¹]	τ	$\int_{\text{FWHM}} I \delta v$ [J beam ⁻¹ km s ⁻¹]	Detection level
31 _{3,28} – 30 _{4,27} EE	334706.67	277	-2.9889	1.12e-01	0.255	71
31 _{4,28} – 30 _{4,27} EE	334706.67	277	-3.2332	6.39e-02	0.255	71
31 _{4,28} – 30 _{3,27} EE	334706.67	277	-2.9889	1.12e-01	0.255	71
31 _{3,28} – 30 _{4,27} AA	334747.64	277	-2.7968	1.10e-01	0.149	42
31 _{3,28} – 30 _{4,27} AA	334747.64	277	-2.7968	1.10e-01	0.160	45
31 _{4,28} – 30 _{3,27} AA	334747.64	277	-2.7969	6.60e-02	0.149	42
31 _{4,28} – 30 _{3,27} AA	334747.64	277	-2.7969	6.60e-02	0.160	45
21 _{13,9} – 20 _{12,8} EE	335150.46	187	-3.3155	7.48e-02	0.059	16
23 _{12,11} – 22 _{13,10} AE	335336.65	219	-3.2138	3.00e-02	0.033	9
23 _{12,11} – 22 _{13,10} EE	335427.63	219	-3.2142	8.00e-02	0.087	24
22 _{13,10} – 21 _{12,9} EE	335617.32	202	-3.2655	7.73e-02	0.075	21
32 _{2,30} – 31 _{3,29} EA	335802.89	281	-2.7724	4.61e-02	0.167	47
32 _{3,30} – 31 _{2,29} EA	335802.89	281	-2.7724	4.61e-02	0.167	47
32 _{2,30} – 31 _{2,29} AE	335802.91	281	-2.7724	6.92e-02	0.167	47
32 _{3,30} – 31 _{3,29} AE	335802.91	281	-2.7724	2.31e-02	0.167	47
32 _{2,30} – 31 _{3,29} EE	335835.06	281	-3.1155	8.05e-02	0.219	61
32 _{2,30} – 31 _{2,29} EE	335835.06	281	-3.0035	1.04e-01	0.219	61
32 _{3,30} – 31 _{3,29} EE	335835.06	281	-3.0035	1.04e-01	0.219	61
32 _{3,30} – 31 _{2,29} EE	335835.06	281	-3.1155	8.05e-02	0.219	61
32 _{3,30} – 31 _{3,29} AA	335867.22	281	-2.7722	6.93e-02	0.156	44
32 _{2,30} – 31 _{2,29} AA	335867.22	281	-2.7722	1.15e-01	0.156	44
15 _{9,7} – 14 _{6,8} EE	335913.15	96	-3.8800	3.03e-02	0.049	14
20 _{13,8} – 19 _{12,7} AE	335925.12	172	-3.3067	3.07e-02	0.013	4
17 _{16,2} – 16 _{15,1} AE	336425.06	142	-2.8089	3.46e-02	0.137	38
17 _{16,1} – 16 _{15,2} AE	336425.21	142	-2.8089	1.04e-01	0.137	38
17 _{16,2} – 16 _{15,2} EA	336499.84	142	-2.8087	6.93e-02	0.116	32
23 _{13,10} – 22 _{14,9} EE	336595.46	222	-3.3730	5.35e-02	0.043	12
17 _{16,1} – 16 _{15,1} EE	336627.03	142	-2.8079	2.77e-01	0.267	75
20 _{13,8} – 19 _{12,7} AA	336659.82	172	-3.3026	5.14e-02	0.019	5
17 _{16,2} – 16 _{15,2} EE	336700.98	142	-2.8077	2.77e-01	0.220	61
24 _{11,13} – 23 _{12,12} EE	336848.82	230	-3.0930	9.95e-02	0.105	29
24 _{12,13} – 23 _{11,12} EA	336881.18	230	-3.0924	2.49e-02	0.036	10
24 _{12,13} – 23 _{11,12} AE	336882.02	230	-3.0924	3.73e-02	0.036	10
17 _{16,2} – 16 _{15,1} AA	336902.73	142	-2.8067	1.04e-01	0.224	62
17 _{16,1} – 16 _{15,2} AA	336902.88	142	-2.8067	1.74e-01	0.224	62
24 _{11,13} – 23 _{12,12} AA	336942.18	230	-3.0931	3.73e-02	0.053	15
33 _{1,32} – 32 _{2,31} EA	336947.69	285	-2.7496	4.84e-02	0.158	44
33 _{2,32} – 32 _{1,31} EA	336947.69	285	-2.7496	4.84e-02	0.158	44
33 _{2,32} – 32 _{2,31} AE	336947.69	285	-2.7496	7.26e-02	0.158	44
33 _{1,32} – 32 _{1,31} AE	336947.69	285	-2.7496	2.42e-02	0.158	44
33 _{1,32} – 32 _{2,31} EE	336968.39	285	-2.8961	1.29e-01	0.221	62
33 _{2,32} – 32 _{2,31} EE	336968.39	285	-3.1937	6.50e-02	0.221	62
33 _{1,32} – 32 _{1,31} EE	336968.39	285	-3.1937	6.50e-02	0.221	62
33 _{2,32} – 32 _{1,31} EE	336968.39	285	-2.8961	1.29e-01	0.221	62
24 _{12,13} – 23 _{11,12} EE	336976.82	230	-3.0925	9.95e-02	0.129	36
33 _{1,32} – 32 _{2,31} AA	336989.07	285	-2.7495	1.21e-01	0.187	52
33 _{2,32} – 32 _{1,31} AA	336989.07	285	-2.7495	7.27e-02	0.187	52
24 _{12,13} – 23 _{11,12} AA	337071.78	230	-3.0924	6.22e-02	0.084	23
25 _{10,15} – 24 _{11,14} EA	337243.77	241	-3.0202	2.80e-02	0.059	16
25 _{10,15} – 24 _{11,14} AE	337243.93	241	-3.0202	4.20e-02	0.087	24
25 _{11,15} – 24 _{10,14} EA	337245.60	241	-3.0202	2.80e-02	0.045	12
25 _{11,15} – 24 _{10,14} AE	337245.77	241	-3.0203	1.40e-02	0.045	12
25 _{10,15} – 24 _{11,14} EE	337325.28	241	-3.0202	1.12e-01	0.060	17
25 _{11,15} – 24 _{10,14} EE	337327.12	241	-3.0202	1.12e-01	0.060	17
25 _{10,15} – 24 _{11,14} AA	337406.52	241	-3.0201	7.00e-02	0.038	11
25 _{11,15} – 24 _{10,14} AA	337408.37	241	-3.0201	4.20e-02	0.038	11
26 _{9,17} – 25 _{10,16} EA	338044.46	251	-2.9640	3.05e-02	0.168	47
26 _{10,17} – 25 _{9,16} EA	338044.48	251	-2.9640	3.05e-02	0.168	47
26 _{9,17} – 25 _{10,16} AE	338044.57	251	-2.9640	1.52e-02	0.168	47

Continued on next page

Table B.1 – continued from previous page

Transition	Frequency [MHz]	E_{up} [K]	$\log_{10}(A_{\text{ul}})$ [s ⁻¹]	τ	$\int_{\text{FWHM}} I \delta v$ [J beam ⁻¹ km s ⁻¹]	Detection level
26 _{10,17} – 25 _{9,16} AE	338044.58	251	-2.9640	4.57e-02	0.168	47
34 _{0,34} – 33 _{1,33} EE	338105.31	288	-3.4554	3.46e-02	0.243	68
34 _{1,34} – 33 _{1,33} EE	338105.31	288	-2.7657	1.69e-01	0.243	68
34 _{0,34} – 33 _{0,33} EE	338105.31	288	-2.7657	1.69e-01	0.243	68
34 _{1,34} – 33 _{0,33} EE	338105.31	288	-3.4554	3.46e-02	0.243	68
34 _{0,34} – 33 _{0,33} AA	338110.81	287	-2.7284	1.27e-01	0.197	55
34 _{1,34} – 33 _{1,33} AA	338110.81	287	-2.7283	7.65e-02	0.197	55
26 _{9,17} – 25 _{10,16} EE	338117.64	251	-2.9640	1.22e-01	0.210	59
26 _{10,17} – 25 _{9,16} EE	338117.66	251	-2.9640	1.22e-01	0.210	59
26 _{9,17} – 25 _{10,16} AA	338190.61	251	-2.9638	4.57e-02	0.114	32
26 _{10,17} – 25 _{9,16} AA	338190.62	251	-2.9638	7.61e-02	0.114	32
18 _{14,5} – 17 _{13,5} EA	338648.66	147	-3.0058	4.43e-02	0.030	8
18 _{14,4} – 17 _{13,4} EE	338833.86	147	-3.0148	1.73e-01	0.148	41
18 _{14,4} – 17 _{13,5} AE	339030.13	147	-2.9994	2.24e-02	0.018	5
27 _{8,19} – 26 _{9,18} EE	339069.60	260	-2.9174	1.30e-01	0.173	48
27 _{9,19} – 26 _{8,18} EE	339069.60	260	-2.9174	1.30e-01	0.173	48
27 _{8,19} – 26 _{9,18} AA	339136.45	260	-2.9173	8.13e-02	0.119	33
27 _{9,19} – 26 _{8,18} AA	339136.45	260	-2.9172	4.88e-02	0.119	33
14 _{5,9} – 13 _{4,10} EE	339242.67	76	-4.2327	1.44e-02	0.032	9
23 _{13,11} – 22 _{12,10} EE	339955.49	219	-3.1917	8.21e-02	0.078	22
28 _{7,21} – 27 _{8,20} EA	340038.58	269	-2.8776	3.44e-02	0.136	38
28 _{8,21} – 27 _{7,20} EA	340038.58	269	-2.8776	3.44e-02	0.136	38
28 _{7,21} – 27 _{8,20} AE	340038.65	269	-2.8777	1.72e-02	0.136	38
28 _{8,21} – 27 _{7,20} AE	340038.65	269	-2.8776	5.16e-02	0.136	38
28 _{7,21} – 27 _{8,20} EE	340100.55	269	-2.8776	1.37e-01	0.187	52
28 _{8,21} – 27 _{7,20} EE	340100.55	269	-2.8776	1.37e-01	0.187	52
28 _{7,21} – 27 _{8,20} AA	340162.36	269	-2.8774	5.16e-02	0.112	31
28 _{8,21} – 27 _{7,20} AA	340162.36	269	-2.8774	8.59e-02	0.112	31
29 _{7,23} – 28 _{7,22} EA	341116.83	276	-2.8426	3.61e-02	0.132	37
29 _{6,23} – 28 _{6,22} EA	341116.83	276	-2.8426	3.61e-02	0.132	37
29 _{6,23} – 28 _{6,22} AE	341116.89	276	-2.8426	1.81e-02	0.132	37
29 _{7,23} – 28 _{7,22} AE	341116.89	276	-2.8426	5.42e-02	0.132	37
29 _{7,23} – 28 _{7,22} EE	341174.15	276	-6.0035	9.97e-05	0.200	56
29 _{6,23} – 28 _{7,22} EE	341174.15	276	-2.8428	1.44e-01	0.200	56
29 _{6,23} – 28 _{6,22} EE	341174.15	276	-6.0035	9.97e-05	0.200	56
29 _{7,23} – 28 _{6,22} EE	341174.15	276	-2.8428	1.44e-01	0.200	56
29 _{6,23} – 28 _{7,22} AA	341231.36	276	-2.8423	9.03e-02	0.132	37
29 _{7,23} – 28 _{6,22} AA	341231.36	276	-2.8424	5.42e-02	0.132	37
44 _{5,39} – 44 _{5,40} EE	341950.48	562	-3.5251	3.21e-03	0.013	4
44 _{6,39} – 44 _{5,40} EE	341950.48	562	-4.1489	7.62e-04	0.013	4
44 _{5,39} – 44 _{4,40} EE	341950.48	562	-4.1489	7.62e-04	0.013	4
44 _{6,39} – 44 _{4,40} EE	341950.48	562	-3.5251	3.21e-03	0.013	4
30 _{6,25} – 29 _{6,24} EA	342219.92	283	-2.8113	3.78e-02	0.124	35
30 _{5,25} – 29 _{5,24} EA	342219.92	283	-2.8113	3.78e-02	0.124	35
30 _{5,25} – 29 _{5,24} AE	342219.97	283	-2.8113	5.67e-02	0.124	35
30 _{6,25} – 29 _{6,24} AE	342219.97	283	-2.8113	1.89e-02	0.124	35
30 _{5,25} – 29 _{6,24} EE	342272.48	283	-3.8339	1.43e-02	0.208	58
30 _{6,25} – 29 _{6,24} EE	342272.48	283	-2.8544	1.37e-01	0.208	58
30 _{5,25} – 29 _{5,24} EE	342272.48	283	-2.8544	1.37e-01	0.208	58
30 _{6,25} – 29 _{5,24} EE	342272.48	283	-3.8339	1.43e-02	0.208	58
17 _{17,1} – 16 _{16,0} AE	342300.57	147	-2.7347	3.83e-02	0.142	40
17 _{17,0} – 16 _{16,1} AE	342300.57	147	-2.7346	1.15e-01	0.142	40
30 _{5,25} – 29 _{6,24} AA	342324.94	283	-2.8110	5.67e-02	0.130	36
30 _{6,25} – 29 _{5,24} AA	342324.94	283	-2.8111	9.45e-02	0.130	36
17 _{17,1} – 16 _{16,1} EA	342410.64	147	-2.7343	7.67e-02	0.095	26
17 _{17,0} – 16 _{16,0} EE	342485.23	147	-2.7339	3.06e-01	0.269	75
17 _{17,1} – 16 _{16,1} EE	342594.89	147	-2.7335	3.07e-01	0.229	64
17 _{17,1} – 16 _{16,0} AA	342780.03	147	-2.7327	1.15e-01	0.227	63
17 _{17,0} – 16 _{16,1} AA	342780.04	147	-2.7328	1.92e-01	0.227	63

Continued on next page

Table B.1 – continued from previous page

Transition	Frequency [MHz]	E_{up} [K]	$\log_{10}(A_{\text{ul}})$ [s ⁻¹]	τ	$\int_{\text{FWHM}} I \delta v$ [J beam ⁻¹ km s ⁻¹]	Detection level
31 _{4,27} – 30 _{5,26} EA	343338.88	289	-2.7830	3.95e-02	0.142	40
31 _{5,27} – 30 _{4,26} EA	343338.88	289	-2.7830	3.95e-02	0.142	40
31 _{4,27} – 30 _{4,26} AE	343338.92	289	-2.7830	1.97e-02	0.142	40
31 _{5,27} – 30 _{5,26} AE	343338.92	289	-2.7830	5.92e-02	0.142	40
31 _{4,27} – 30 _{5,26} AA	343433.08	289	-2.7828	9.87e-02	0.172	48
31 _{5,27} – 30 _{4,26} AA	343433.08	289	-2.7828	5.92e-02	0.172	48
32 _{3,29} – 31 _{4,28} EA	344468.95	294	-2.7572	4.12e-02	0.114	32
32 _{4,29} – 31 _{3,28} EA	344468.95	294	-2.7572	4.12e-02	0.114	32
32 _{4,29} – 31 _{4,28} AE	344468.98	294	-2.7572	2.06e-02	0.114	32
32 _{3,29} – 31 _{3,28} AE	344468.98	294	-2.7572	6.19e-02	0.114	32
32 _{3,29} – 31 _{3,28} EE	344509.42	294	-3.7739	1.52e-02	0.182	51
32 _{3,29} – 31 _{4,28} EE	344509.42	294	-2.7817	1.50e-01	0.182	51
32 _{4,29} – 31 _{3,28} EE	344509.42	294	-2.7817	1.50e-01	0.182	51
32 _{4,29} – 31 _{4,28} EE	344509.42	294	-3.7739	1.52e-02	0.182	51
32 _{3,29} – 31 _{4,28} AA	344549.87	294	-2.7569	6.19e-02	0.181	51
32 _{4,29} – 31 _{3,28} AA	344549.87	294	-2.7570	1.03e-01	0.181	51
18 _{15,3} – 17 _{14,3} EE	345037.50	151	-2.8914	2.16e-01	0.142	40
18 _{15,4} – 17 _{14,4} EE	345073.72	151	-2.8917	2.15e-01	0.210	59
33 _{3,31} – 32 _{3,30} EA	345607.71	298	-2.7333	4.31e-02	0.183	51
33 _{2,31} – 32 _{2,30} EA	345607.71	298	-2.7333	4.31e-02	0.183	51
33 _{3,31} – 32 _{3,30} AE	345607.74	298	-2.7334	6.46e-02	0.183	51
33 _{2,31} – 32 _{2,30} AE	345607.74	298	-2.7334	2.15e-02	0.183	51
33 _{2,31} – 32 _{3,30} EE	345639.62	298	-3.5454	2.48e-02	0.200	56
33 _{2,31} – 32 _{2,30} EE	345639.62	298	-2.7700	1.48e-01	0.200	56
33 _{3,31} – 32 _{3,30} EE	345639.62	298	-2.7700	1.48e-01	0.200	56
33 _{3,31} – 32 _{2,30} EE	345639.62	298	-3.5454	2.48e-02	0.200	56
33 _{2,31} – 32 _{2,30} AA	345671.52	298	-2.7332	6.47e-02	0.140	39
33 _{3,31} – 32 _{3,30} AA	345671.52	298	-2.7332	1.08e-01	0.140	39
25 _{11,14} – 24 _{12,13} EA	346346.12	247	-3.0311	2.48e-02	0.078	22
25 _{11,14} – 24 _{12,13} AE	346346.31	247	-3.0310	3.72e-02	0.078	22
25 _{12,14} – 24 _{11,13} EA	346374.84	247	-3.0309	2.48e-02	0.042	12
25 _{12,14} – 24 _{11,13} AE	346375.23	247	-3.0310	1.24e-02	0.042	12
25 _{11,14} – 24 _{12,13} EE	346432.88	247	-3.0311	9.90e-02	0.091	25
25 _{12,14} – 24 _{11,13} EE	346461.91	247	-3.0310	9.90e-02	0.068	19
25 _{11,14} – 24 _{12,13} AA	346519.31	247	-3.0311	6.19e-02	0.042	12
25 _{12,14} – 24 _{11,13} AA	346548.56	247	-3.0309	3.71e-02	0.067	19
34 _{1,33} – 33 _{2,32} AA	346795.27	301	-2.7111	6.78e-02	0.097	27
34 _{2,33} – 33 _{1,32} AA	346795.27	301	-2.7112	1.13e-01	0.097	27
26 _{10,16} – 25 _{11,15} EA	346941.16	258	-2.9664	2.73e-02	0.081	23
26 _{10,16} – 25 _{11,15} AE	346941.30	258	-2.9664	1.37e-02	0.081	23
26 _{11,16} – 25 _{10,15} EA	346941.51	258	-2.9664	2.73e-02	0.081	23
26 _{11,16} – 25 _{10,15} AE	346941.65	258	-2.9664	4.09e-02	0.081	23
26 _{10,16} – 25 _{11,15} EE	347017.52	258	-2.9663	1.09e-01	0.142	40
26 _{11,16} – 25 _{10,15} EE	347017.87	258	-2.9663	1.09e-01	0.142	40
26 _{10,16} – 25 _{11,15} AA	347093.62	258	-2.9662	4.09e-02	0.101	28
26 _{11,16} – 25 _{10,15} AA	347093.97	258	-2.9663	6.82e-02	0.101	28
24 _{13,12} – 23 _{12,11} EE	347309.14	235	-3.1182	8.51e-02	0.099	28
27 _{9,18} – 26 _{10,17} EA	347797.75	268	-2.9148	2.93e-02	0.138	39
27 _{10,18} – 26 _{9,17} EA	347797.75	268	-2.9148	2.93e-02	0.138	39
27 _{9,18} – 26 _{10,17} AE	347797.85	268	-2.9148	4.40e-02	0.138	39
27 _{10,18} – 26 _{9,17} AE	347797.85	268	-2.9148	1.47e-02	0.138	39
27 _{9,18} – 26 _{10,17} EE	347867.07	268	-2.9147	1.17e-01	0.186	52
27 _{10,18} – 26 _{9,17} EE	347867.08	268	-2.9147	1.17e-01	0.186	52
35 _{0,35} – 34 _{1,34} AE	347907.80	304	-2.6907	7.10e-02	0.130	36
35 _{1,35} – 34 _{0,34} AE	347907.80	304	-2.6907	2.37e-02	0.130	36
35 _{0,35} – 34 _{1,34} EA	347907.85	304	-2.6907	4.73e-02	0.130	36
35 _{1,35} – 34 _{0,34} EA	347907.85	304	-2.6907	4.73e-02	0.130	36
35 _{0,35} – 34 _{1,34} AA	347918.78	304	-2.6907	1.18e-01	0.133	37
35 _{1,35} – 34 _{0,34} AA	347918.78	304	-2.6907	7.11e-02	0.133	37

Continued on next page

Table B.1 – continued from previous page

Transition	Frequency [MHz]	E_{up} [K]	$\log_{10}(A_{\text{ul}})$ [s ⁻¹]	τ	$\int_{\text{FWHM}} I \delta v$ [J beam ⁻¹ km s ⁻¹]	Detection level
27 _{9,18} – 26 _{10,17} AA	347936.19	268	-2.9146	7.33e-02	0.085	24
27 _{10,18} – 26 _{9,17} AA	347936.20	268	-2.9145	4.40e-02	0.085	24
28 _{8,20} – 27 _{9,19} EA	348780.22	277	-2.8714	3.10e-02	0.092	26
28 _{9,20} – 27 _{8,19} EA	348780.22	277	-2.8714	3.10e-02	0.092	26
28 _{8,20} – 27 _{9,19} AE	348780.29	277	-2.8713	1.55e-02	0.092	26
28 _{9,20} – 27 _{8,19} AE	348780.29	277	-2.8714	4.65e-02	0.092	26
28 _{8,20} – 27 _{9,19} EE	348844.27	277	-2.8712	1.24e-01	0.144	40
28 _{9,20} – 27 _{8,19} EE	348844.27	277	-2.8712	1.24e-01	0.144	40
28 _{8,20} – 27 _{9,19} AA	348908.15	277	-2.8711	4.65e-02	0.097	27
28 _{9,20} – 27 _{8,19} AA	348908.15	277	-2.8711	7.76e-02	0.097	27
14 _{4,10} – 13 _{3,11} EE	348964.09	72	-4.4168	9.23e-03	0.014	4
14 _{5,10} – 13 _{2,11} EE	348964.42	72	-4.4168	9.23e-03	0.014	4
29 _{7,22} – 28 _{8,21} EA	349827.76	285	-2.8337	3.26e-02	0.120	34
29 _{8,22} – 28 _{7,21} EA	349827.76	285	-2.8337	3.26e-02	0.120	34
29 _{7,22} – 28 _{8,21} AE	349827.82	285	-2.8338	4.89e-02	0.120	34
29 _{8,22} – 28 _{7,21} AE	349827.82	285	-2.8338	1.63e-02	0.120	34
29 _{8,22} – 28 _{8,21} EE	349887.43	285	-2.8633	1.22e-01	0.150	42
29 _{7,22} – 28 _{8,21} EE	349887.43	285	-4.0142	8.60e-03	0.150	42
29 _{7,22} – 28 _{7,21} EE	349887.43	285	-2.8631	1.22e-01	0.150	42
29 _{8,22} – 28 _{7,21} EE	349887.43	285	-4.0172	8.54e-03	0.150	42
29 _{7,22} – 28 _{8,21} AA	349946.96	285	-2.8335	8.14e-02	0.100	28
29 _{8,22} – 28 _{7,21} AA	349946.96	285	-2.8334	4.89e-02	0.100	28
18 _{16,3} – 17 _{15,2} AE	350819.12	155	-2.8044	9.25e-02	0.070	19
18 _{16,2} – 17 _{15,3} AE	350821.27	155	-2.8044	3.08e-02	0.015	4
18 _{16,3} – 17 _{15,3} EA	350891.89	155	-2.8043	6.17e-02	0.047	13
30 _{6,24} – 29 _{6,23} EA	350911.96	293	-2.8004	3.40e-02	0.118	33
30 _{7,24} – 29 _{7,23} EA	350911.96	293	-2.8004	3.40e-02	0.118	33
30 _{6,24} – 29 _{6,23} AE	350912.01	293	-2.8004	5.10e-02	0.118	33
30 _{7,24} – 29 _{7,23} AE	350912.01	293	-2.8004	1.70e-02	0.118	33
30 _{6,24} – 29 _{6,23} EE	350967.54	293	-3.4934	2.76e-02	0.187	52
30 _{6,24} – 29 _{7,23} EE	350967.54	293	-2.8987	1.09e-01	0.187	52
30 _{7,24} – 29 _{7,23} EE	350967.54	293	-3.2594	4.73e-02	0.187	52
30 _{7,24} – 29 _{6,23} EE	350967.54	293	-2.9856	8.88e-02	0.187	52
18 _{16,2} – 17 _{15,2} EE	351012.48	155	-2.8033	2.47e-01	0.214	60
30 _{7,24} – 29 _{7,23} AA	351023.02	293	-2.8002	5.10e-02	0.111	31
30 _{6,24} – 29 _{6,23} AA	351023.02	293	-2.8002	8.51e-02	0.111	31
18 _{16,3} – 17 _{15,3} EE	351083.30	155	-2.8032	2.47e-01	0.182	51
18 _{16,3} – 17 _{15,2} AA	351274.14	155	-2.8021	1.55e-01	0.115	32
31 _{5,26} – 30 _{5,25} EA	352018.43	300	-2.7706	3.55e-02	0.135	38
31 _{6,26} – 30 _{6,25} EA	352018.43	300	-2.7706	3.55e-02	0.135	38
31 _{5,26} – 30 _{6,25} AE	352018.48	300	-2.7706	5.32e-02	0.135	38
31 _{6,26} – 30 _{5,25} AE	352018.48	300	-2.7705	1.77e-02	0.135	38
31 _{5,26} – 30 _{6,25} EE	352069.73	300	-5.6440	1.88e-04	0.187	52
31 _{5,26} – 30 _{5,25} EE	352069.73	300	-2.7671	1.42e-01	0.187	52
31 _{6,26} – 30 _{6,25} EE	352069.73	300	-2.7671	1.42e-01	0.187	52
31 _{6,26} – 30 _{5,25} EE	352069.73	300	-5.6440	1.88e-04	0.187	52
31 _{5,26} – 30 _{5,25} AA	352120.94	300	-2.7703	5.32e-02	0.136	38
31 _{6,26} – 30 _{6,25} AA	352120.94	300	-2.7703	8.87e-02	0.136	38
24 _{13,11} – 23 _{14,10} EE	352593.82	239	-3.2028	6.58e-02	0.080	22
19 _{14,6} – 18 _{13,6} EA	352777.63	161	-3.1271	2.93e-02	0.033	9
16 _{11,6} – 15 _{8,7} EE	352842.59	113	-3.8606	2.68e-02	0.035	10
16 _{11,6} – 15 _{8,7} EE	352842.59	113	-3.8606	2.68e-02	0.029	8
32 _{4,28} – 31 _{5,27} EA	353139.60	306	-2.7434	3.69e-02	0.116	32
32 _{5,28} – 31 _{4,27} EA	353139.60	306	-2.7434	3.69e-02	0.116	32
32 _{4,28} – 31 _{4,27} AE	353139.65	306	-2.7434	5.54e-02	0.116	32
32 _{5,28} – 31 _{5,27} AE	353139.65	306	-2.7433	1.85e-02	0.116	32
32 _{4,28} – 31 _{4,27} EE	353185.88	306	-2.7258	1.48e-01	0.185	52
32 _{5,28} – 31 _{5,27} EE	353185.88	306	-2.7258	1.48e-01	0.185	52
32 _{4,28} – 31 _{5,27} AA	353232.11	306	-2.7431	5.54e-02	0.114	32

Continued on next page

Table B.1 – continued from previous page

Transition	Frequency [MHz]	E_{up} [K]	$\log_{10}(A_{\text{ul}})$ [s ⁻¹]	τ	$\int_{\text{FWHM}} I \delta v$ [J beam ⁻¹ km s ⁻¹]	Detection level
32 _{5,28} – 31 _{4,27} AA	353232.11	306	-2.7432	9.23e-02	0.114	32
16 _{10,7} – 15 _{7,8} EE	353644.50	110	-3.7796	3.29e-02	0.061	17
16 _{10,7} – 15 _{7,8} AA	353896.48	110	-3.7790	2.06e-02	0.033	9
33 _{3,30} – 32 _{4,29} EA	354271.40	311	-2.7185	3.84e-02	0.171	48
33 _{4,30} – 32 _{3,29} EA	354271.40	311	-2.7185	3.84e-02	0.171	48
33 _{3,30} – 32 _{3,29} AE	354271.44	311	-2.7185	1.92e-02	0.171	48
33 _{4,30} – 32 _{4,29} AE	354271.44	311	-2.7185	5.76e-02	0.171	48
19 _{14,5} – 18 _{13,6} AE	354307.91	161	-3.0237	5.52e-02	0.033	9
33 _{3,30} – 32 _{4,29} EE	354311.36	311	-3.6682	1.61e-02	0.269	75
33 _{3,30} – 32 _{3,29} EE	354311.36	311	-2.7358	1.38e-01	0.269	75
33 _{4,30} – 32 _{4,29} EE	354311.36	311	-2.7358	1.38e-01	0.269	75
33 _{4,30} – 32 _{3,29} EE	354311.36	311	-3.6682	1.61e-02	0.269	75
33 _{3,30} – 32 _{4,29} AA	354351.30	311	-2.7183	9.61e-02	0.176	49
33 _{4,30} – 32 _{3,29} AA	354351.30	311	-2.7183	5.77e-02	0.176	49
34 _{2,32} – 33 _{3,31} EA	355411.74	315	-2.6955	4.00e-02	0.129	36
34 _{3,32} – 33 _{2,31} EA	355411.74	315	-2.6955	4.00e-02	0.129	36
34 _{2,32} – 33 _{3,31} AE	355411.77	315	-2.6955	6.00e-02	0.129	36
34 _{3,32} – 33 _{3,31} AE	355411.77	315	-2.6955	2.00e-02	0.129	36
34 _{3,32} – 33 _{3,31} EE	355443.39	315	-2.6521	1.60e-01	0.201	56
34 _{2,32} – 33 _{2,31} EE	355443.39	315	-2.6521	1.60e-01	0.201	56
34 _{3,32} – 33 _{3,31} AA	355475.05	315	-2.6953	6.01e-02	0.239	67
34 _{2,32} – 33 _{2,31} AA	355475.05	315	-2.6953	1.00e-01	0.239	67
25 _{12,13} – 24 _{13,12} AE	355620.72	252	-3.0519	3.23e-02	0.053	15
25 _{12,13} – 24 _{13,12} EA	355621.08	252	-3.0519	2.15e-02	0.053	15
25 _{12,13} – 24 _{13,12} EE	355713.67	252	-3.0520	8.60e-02	0.092	26
25 _{12,13} – 24 _{13,12} AA	355806.17	252	-3.0520	5.37e-02	0.040	11
26 _{12,15} – 25 _{11,14} EA	355972.75	264	-2.9740	2.43e-02	0.064	18
26 _{12,15} – 25 _{11,14} AE	355972.99	264	-2.9740	3.64e-02	0.064	18
26 _{11,15} – 25 _{12,14} EE	356046.79	264	-2.9739	9.71e-02	0.110	31
26 _{12,15} – 25 _{11,14} EE	356052.97	264	-2.9739	9.71e-02	0.107	30
25 _{13,13} – 24 _{12,12} EE	356066.12	252	-3.0504	8.61e-02	0.124	35
26 _{12,15} – 25 _{11,14} AA	356132.86	264	-2.9739	6.07e-02	0.057	16
35 _{1,34} – 34 _{1,33} EA	356559.73	319	-2.6741	4.18e-02	0.127	35
35 _{2,34} – 34 _{2,33} EA	356559.73	319	-2.6741	4.18e-02	0.127	35
35 _{1,34} – 34 _{1,33} AE	356559.73	319	-2.6741	2.09e-02	0.127	35
35 _{2,34} – 34 _{2,33} AE	356559.73	319	-2.6740	6.27e-02	0.127	35
35 _{1,34} – 34 _{2,33} EE	356580.23	319	-2.6206	1.66e-01	0.196	55
35 _{2,34} – 34 _{2,33} EE	356580.23	319	-4.8932	8.88e-04	0.196	55
35 _{1,34} – 34 _{1,33} EE	356580.23	319	-4.8932	8.88e-04	0.196	55
35 _{2,34} – 34 _{1,33} EE	356580.23	319	-2.6206	1.66e-01	0.196	55
35 _{1,34} – 34 _{2,33} AA	356600.73	319	-2.6740	1.05e-01	0.128	36
35 _{2,34} – 34 _{1,33} AA	356600.73	319	-2.6740	6.28e-02	0.128	36
18 _{17,1} – 17 _{16,1} EA	356621.39	160	-2.7275	6.88e-02	0.065	18
27 _{10,17} – 26 _{11,16} EA	356658.41	275	-2.9156	2.63e-02	0.112	31
27 _{11,17} – 26 _{10,16} EA	356658.48	275	-2.9156	2.63e-02	0.112	31
27 _{10,17} – 26 _{11,16} AE	356658.54	275	-2.9156	3.95e-02	0.112	31
27 _{11,17} – 26 _{10,16} AE	356658.60	275	-2.9156	1.32e-02	0.112	31
18 _{17,2} – 17 _{16,1} AE	356727.49	159	-2.7272	1.03e-01	0.070	20
18 _{17,1} – 17 _{16,2} AE	356727.54	159	-2.7272	3.44e-02	0.070	20
27 _{10,17} – 26 _{11,16} AA	356801.31	275	-2.9153	6.58e-02	0.097	27
27 _{11,17} – 26 _{10,16} AA	356801.37	275	-2.9154	3.95e-02	0.097	27
18 _{17,2} – 17 _{16,2} EA	356833.46	159	-2.7269	6.89e-02	0.078	22
18 _{17,1} – 17 _{16,1} EE	356902.77	160	-2.7263	2.75e-01	0.193	54
18 _{17,2} – 17 _{16,2} EE	357008.08	159	-2.7261	2.76e-01	0.289	81
18 _{17,2} – 17 _{16,1} AA	357183.43	160	-2.7252	1.72e-01	0.225	63
18 _{17,1} – 17 _{16,2} AA	357183.48	160	-2.7253	1.03e-01	0.225	63
28 _{9,19} – 27 _{10,18} EA	357558.00	285	-2.8678	2.80e-02	0.106	30
28 _{10,19} – 27 _{9,18} EA	357558.01	285	-2.8678	2.80e-02	0.106	30
28 _{9,19} – 27 _{10,18} AE	357558.09	285	-2.8678	1.40e-02	0.106	30

Continued on next page

Table B.1 – continued from previous page

Transition	Frequency [MHz]	E_{up} [K]	$\log_{10}(A_{\text{ul}})$ [s ⁻¹]	τ	$\int_{\text{FWHM}} I \delta v$ [J beam ⁻¹ km s ⁻¹]	Detection level
28 _{10,19} – 27 _{9,18} AE	357558.09	285	-2.8678	4.20e-02	0.106	30
28 _{9,19} – 27 _{10,18} EE	357623.66	285	-2.8677	1.12e-01	0.182	51
28 _{10,19} – 27 _{9,18} EE	357623.66	285	-2.8677	1.12e-01	0.182	51
28 _{9,19} – 27 _{10,18} AA	357689.11	285	-2.8675	4.20e-02	0.127	35
28 _{10,19} – 27 _{9,18} AA	357689.11	285	-2.8676	6.99e-02	0.127	35
36 _{0,36} – 35 _{0,35} AE	357715.22	322	-2.6541	6.56e-02	0.154	43
36 _{1,36} – 35 _{1,35} AE	357715.22	322	-2.6541	2.19e-02	0.154	43
36 _{0,36} – 35 _{1,35} EA	357715.27	322	-2.6541	4.37e-02	0.154	43
36 _{1,36} – 35 _{0,35} EA	357715.27	322	-2.6541	4.37e-02	0.154	43
36 _{0,36} – 35 _{1,35} EE	357720.70	321	-2.5866	1.75e-01	0.235	66
36 _{1,36} – 35 _{1,35} EE	357720.70	321	-5.6153	1.64e-04	0.235	66
36 _{1,36} – 35 _{0,35} EE	357720.70	321	-2.5866	1.75e-01	0.235	66
36 _{0,36} – 35 _{0,35} EE	357720.70	321	-5.6153	1.64e-04	0.235	66
36 _{0,36} – 35 _{1,35} AA	357726.06	321	-2.6541	6.57e-02	0.155	43
36 _{1,36} – 35 _{0,35} AA	357726.06	321	-2.6541	1.09e-01	0.155	43
29 _{8,21} – 28 _{9,20} EA	358560.03	294	-2.8271	2.94e-02	0.126	35
29 _{9,21} – 28 _{8,20} EA	358560.03	294	-2.8271	2.94e-02	0.126	35
29 _{8,21} – 28 _{9,20} AE	358560.10	294	-2.8271	4.41e-02	0.126	35
29 _{9,21} – 28 _{8,20} AE	358560.10	294	-2.8270	1.47e-02	0.126	35
29 _{8,21} – 28 _{9,20} EE	358621.21	294	-2.8269	1.18e-01	0.195	55
29 _{9,21} – 28 _{8,20} EE	358621.21	294	-2.8269	1.18e-01	0.195	55
29 _{8,21} – 28 _{9,20} AA	358682.23	294	-2.8268	7.34e-02	0.118	33
29 _{9,21} – 28 _{8,20} AA	358682.23	294	-2.8268	4.41e-02	0.118	33
19 _{15,5} – 18 _{14,5} EA	359063.67	164	-2.9024	4.61e-02	0.052	15
19 _{15,4} – 18 _{14,4} EE	359225.22	164	-2.9025	1.84e-01	0.159	44
19 _{15,5} – 18 _{14,5} EE	359266.93	164	-2.9031	1.84e-01	0.142	40
30 _{8,23} – 29 _{8,22} EA	359617.24	303	-2.7914	3.07e-02	0.119	33
30 _{7,23} – 29 _{7,22} EA	359617.24	303	-2.7914	3.07e-02	0.119	33
30 _{7,23} – 29 _{8,22} AE	359617.31	303	-2.7914	1.53e-02	0.119	33
30 _{8,23} – 29 _{7,22} AE	359617.31	303	-2.7914	4.60e-02	0.119	33
30 _{7,23} – 29 _{8,22} EE	359674.69	303	-4.9449	8.61e-04	0.163	45
30 _{8,23} – 29 _{8,22} EE	359674.69	303	-2.7943	1.22e-01	0.163	45
30 _{8,23} – 29 _{7,22} EE	359674.69	303	-4.9449	8.61e-04	0.163	45
30 _{7,23} – 29 _{7,22} EE	359674.69	303	-2.7943	1.22e-01	0.163	45
30 _{8,23} – 29 _{8,22} AA	359731.98	303	-2.7912	4.60e-02	0.100	28
30 _{8,23} – 29 _{8,22} AA	359731.98	303	-2.7912	4.60e-02	0.102	28
30 _{7,23} – 29 _{7,22} AA	359731.98	303	-2.7911	7.67e-02	0.100	28
30 _{7,23} – 29 _{7,22} AA	359731.98	303	-2.7911	7.67e-02	0.102	28
31 _{6,25} – 30 _{7,24} EA	360706.63	310	-2.7597	3.19e-02	0.152	42
31 _{7,25} – 30 _{6,24} EA	360706.63	310	-2.7597	3.19e-02	0.152	42
31 _{6,25} – 30 _{7,24} AE	360706.68	310	-2.7597	4.78e-02	0.152	42
31 _{7,25} – 30 _{6,24} AE	360706.68	310	-2.7597	1.59e-02	0.152	42
31 _{7,25} – 30 _{7,24} EE	360760.53	310	-2.7647	1.25e-01	0.175	49
31 _{6,25} – 30 _{7,24} EE	360760.53	310	-4.4450	2.61e-03	0.175	49
31 _{6,25} – 30 _{6,24} EE	360760.53	310	-2.7559	1.27e-01	0.175	49
31 _{7,25} – 30 _{6,24} EE	360760.53	310	-6.1629	4.99e-05	0.175	49
31 _{6,25} – 30 _{6,24} AA	360814.30	310	-2.7595	4.78e-02	0.097	27
31 _{7,25} – 30 _{7,24} AA	360814.30	310	-2.7594	7.97e-02	0.097	27
23 _{14,10} – 22 _{13,9} EE	360915.54	223	-3.2141	6.73e-02	0.088	25
32 _{6,27} – 31 _{6,26} EA	361816.20	317	-2.7310	3.31e-02	0.155	43
32 _{5,27} – 31 _{5,26} EA	361816.20	317	-2.7310	3.31e-02	0.155	43
32 _{5,27} – 31 _{5,26} AE	361816.25	317	-2.7310	4.96e-02	0.155	43
32 _{6,27} – 31 _{6,26} AE	361816.25	317	-2.7311	1.65e-02	0.155	43
32 _{5,27} – 31 _{6,26} EE	361866.27	317	-2.7219	1.30e-01	0.204	57
32 _{6,27} – 31 _{6,26} EE	361866.27	317	-4.4333	2.52e-03	0.204	57
32 _{5,27} – 31 _{5,26} EE	361866.27	317	-4.4333	2.52e-03	0.204	57
32 _{6,27} – 31 _{5,26} EE	361866.27	317	-2.7219	1.30e-01	0.204	57
32 _{5,27} – 31 _{6,26} AA	361916.24	317	-2.7308	4.96e-02	0.133	37
32 _{6,27} – 31 _{5,26} AA	361916.24	317	-2.7308	8.27e-02	0.133	37

Continued on next page

Table B.1 – continued from previous page

Transition	Frequency [MHz]	E_{up} [K]	$\log_{10}(A_{\text{ul}})$ [s ⁻¹]	τ	$\int_{\text{FWHM}} I \delta v$ [J beam ⁻¹ km s ⁻¹]	Detection level
24 _{14,11} – 23 _{13,10} EE	362230.43	240	-3.1534	6.99e-02	0.063	18
18 _{18,0} – 17 _{17,0} EA	362458.25	164	-2.6580	7.52e-02	0.061	17
18 _{18,1} – 17 _{17,0} AE	362600.03	164	-2.6576	1.13e-01	0.154	43
18 _{18,0} – 17 _{17,1} AE	362600.03	164	-2.6576	3.76e-02	0.154	43
18 _{18,1} – 17 _{17,1}	362741.13	164	-2.6571	7.54e-02	0.173	48
18 _{18,0} – 17 _{17,0} EE	362755.32	164	-2.6569	3.01e-01	0.239	67
16 _{9,8} – 15 _{6,9} EA	362811.49	107	-3.8228	7.25e-03	0.019	5

Table C.1: Acetone lines with high K_a and low K_c quantum numbers

Transition	Predicted frequency [MHz]
$19_{13,7} - 18_{12,6}$ EE	334948.01
$18_{13,5} - 17_{12,6}$ EE	336133.79
$18_{14,5} - 17_{13,4}$ AE	338242.61
$18_{14,4} - 17_{13,4}$ EA	338625.87
$18_{14,4} - 17_{13,5}$ AA	339459.74
$18_{12,6} - 17_{11,7}$ EE	342896.39
$18_{15,3} - 17_{14,3}$ EA	344793.57
$19_{14,6} - 18_{13,5}$ EE	350205.27
$19_{14,6} - 18_{13,5}$ AA	351215.21
$19_{14,6} - 18_{13,6}$ EE	353155.67
$19_{14,5} - 18_{13,6}$ AA	354673.02
$19_{14,5} - 18_{13,6}$ EE	355248.54
$19_{13,6} - 18_{12,7}$ AA	356644.96
$19_{13,6} - 18_{12,7}$ EE	356675.20
$19_{15,4} - 18_{14,5}$ AE	359197.90
$19_{15,5} - 18_{14,4}$ AA	359301.10
$20_{14,7} - 19_{13,6}$ EE	359843.80
$20_{14,7} - 19_{13,6}$ AA	360338.51

Notes. These acetone lines appear missing or shifted when comparing the synthetic spectrum with the observed spectrum. This could be due to perturbations by interactions between the (high K_a , low K_c) levels and the levels from the lowest torsional excited states (Groner et al. 2002).

Appendix C: Acetone lines with high K_a and low K_c quantum numbers